Structural Effects on the Isomerization Dynamics of *trans*-Stilbenes: IVR, Microcanonical Reaction Rates, and the Nature of the Transition State

A. A. Heikal, J. S. Baskin, L. Bañares,† and A. H. Zewail*

Arthur Amos Noyes Laboratory of Chemical Physics, California Institute of Technology, Pasadena, California 91125

Received: July 2, 1996; In Final Form: September 2, 1996[⊗]

Picosecond time-resolved fluorescence spectroscopy has been used for studying the intramolecular dynamics of *trans*-stilbene (TS) derivatives. Nonradiative decay rate constants (k_{nr}) of jet-cooled 4-methoxy-*trans*-stilbene (MS), 4,4′-dimethoxy-*trans*-stilbene (DMS), 2-phenylindene (PI), 4,4′-dihydroxy-*trans*-stilbene (DHS), and 1-(*trans*-β-styryl)cyclohexene (SCH) have been obtained from time-resolved fluorescence measurements with wide-band detection from photoselected vibrational states in the S_1 manifold. Time- and frequency-resolved fluorescence have been measured to characterize intramolecular vibrational energy redistribution (IVR) in the first three of these molecules. Statistical nonadiabatic RRKM theory is applied to model the energy dependence of k_{nr} and extract the reaction barriers. Dispersed fluorescence is measured and analyzed in order to determine the substitution effect on vibrational frequencies most significant to the RRKM calculations. While k_{nr} is almost invariant to *para* substitution of a methoxy group, with similar isomerization thresholds for MS and TS ($E_0^{MS} \sim E_0^{TS}$), a dramatic slowing of the rate is observed in both disubstituted derivatives, and reaction barriers of ∼1800 and 1700 cm^{-1} are derived for DMS and DHS, respectively. The altered conjugation of the system in SCH produces a large blue shift of the 0_0^0 and results in a lowering of the isomerization barrier ($E_0^{SCH} < 740$ cm^{-1}). The twisting around the ethylenic double bond (C_e-C_e) is prevented upon intramolecular bridging in PI, but another nonradiative channel, attributed to twisting around the C_e-C_φ single bond, is modeled by RRKM theory with $E_0^{PI} \sim 1770$ cm^{-1}. From the electronic structure effects on both E_0 and the shift of the S_1 transition, we elucidate the nature of the transition state, as *zwitterionic*, and we correlate substitution effects with the HOMO/LUMO (frontier orbital) description. The results are relevant to studies in polar solutions and to the dimensionality of the reaction coordinate in the dynamics of barrier crossing.

I. Introduction

The photoisomerization reaction of *trans*-stilbene is one of the most extensively studied photochemical reactions and has generated a vast literature. (For recent reviews see refs 1 and 2.) The photoisomerization process has been found to proceed by overcoming an energy barrier (E_0) of about ∼1200 cm^{-1} in supersonic jet expansions using picosecond time-resolved fluorescence spectroscopy.[3−8] Theoretically, Orlandi and Siebrand[9] developed a model in which the photoisomerization is produced by a nonadiabatic crossing between the potential energy curves for twisting of the ethylene bond of two excited singlet electronic states, the higher of which has a minimum at the perpendicular configuration (*phantom* state). Quantum chemical calculations by Tavan *et al*.,[10] Orlandi *et al*.,[11] Olbrich,[12] and Hohlneicher *et al*.[13] agree, in general, with this photoisomerization mechanism.

Comparisons of the excess energy dependence of the photoisomerization rate constant with the RRKM theory of unimolecular reactions have been made for over a decade,[5,6,8,14−17] with a primary focus resting on the extent of vibrational energy randomization and the nature of the transition state. Recently,[17] with the extension of the experimental investigation of *trans*-stilbene dynamics into the femtosecond time domain, it was shown that the entire body of available experimental data on photoisomerization of isolated *trans*-stilbene is well represented by RRKM theory (modified to take into account the unique nature of the transition state) based on semiempirical reactant and transition state vibrational frequencies.[16] The indications that intramolecular vibrational energy redistribution (IVR) occurs on the subpicosecond or shorter time scale (∼100 times faster than isomerization at comparable excess energy) and the well-known fact that photoisomerization depends only on the total vibrational energy[5,18] support the assumption that IVR is not the rate-determining step above the isomerization barrier and that statistical theories should be applicable.

One means of further addressing the role of vibrational energy randomization and the nature of the transition state is through the study of the effects of chemical substituents on the rate constants. Remotely attached substituents introduce additional vibrational degrees of freedom which, when assumed to participate fully in the reactant bath, have a major effect on statistical theory rates via substantial contributions to the vibrational state density. They may also alter the potential surfaces on which the reaction proceeds, affecting the energetics and transition state properties. In an early example of this approach, Jortner *et al*. studied the photoisomerization of 4-alkyl-*trans*-stilbenes (alkyl = methyl, ethyl, and propyl) and 4-chloro-*trans*-stilbene in supersonic jets by picosecond time-resolved fluorescence spectroscopy.[4,7] The photoisomerization rates were almost the same for methyl and chloro substitutions in comparison with *trans*-stilbene and increased somewhat in 4-ethyl- and 4-propyl-*trans*-stilbene. Although this result is in conflict with the predicted rate reduction from a pure state density effect,[15] Jortner and co-workers concluded that consistency with RRKM theory could be preserved if the photo-

† Fulbright/M.E.C. of Spain Postdoctoral Fellow. Present address: Departamento de Química Física, Facultad de Química, Universidad Complutense de Madrid, 28040 Madrid, Spain.

⊗ Abstract published in *Advance ACS Abstracts,* January 1, 1997.

S1089-5639(96)01971-8 CCC: $14.00

isomerization threshold is lowered by substitution (by ~100, 200, and 300 cm^{-1} for 4-methyl-, 4-ethyl-, and 4-propyl-*trans*-stilbene, respectively[7]).

More recently, a comparison of the dynamics (IVR and photoisomerization), measured via picosecond time-resolved fluorescence of jet-cooled samples, of a series of *trans*-stilbene (TS) derivatives was reported from this lab: 4-methoxy-*trans*-stilbene (MS), 4,4′-dimethoxy-*trans*-stilbene (DMS), and a bridged derivative, 2-phenylindene (PI).[19] In the case of the last molecule, PI, the ethylenic (C_e-C_e double bond) twisting isomerization channel is closed by intramolecular bridging, and the observed nonradiative rate is interpreted as representing the contribution of the twisting motion around the unbridged C_e-C_φ bond. The energy dependence of k_{nr} was found to decrease very slightly for *para* substitution of a methoxy group, while a dramatic change in rate was observed with a second methoxy group in the complementary *para* position, and for PI. In the preliminary report of this work, values of E_0 were estimated for each molecule by the point at which the nonradiative rate matched that measured for *trans*-stilbene at its threshold of 1200 cm^{-1}, as determined by fits to RRKM theory.[6,16]

The photoisomerization of a number of disubstituted stilbenes in solution has been extensively studied by Waldeck and associates.[20−27] In the most recent and extensive analysis of available data on 4,4′-dimethyl-*trans*-stilbene, 4,4′-di-*tert*-butyl-*trans*-stilbene, and 4,4′-dimethoxy-*trans*-stilbene in *n*-alkane solvents,[27] the intrinsic (i.e., extrapolated to zero viscosity) enthalpies of activation of the isomerization reaction, $\Delta H_t^‡$, were extracted from the viscosity dependence of the thermal rate constants using the medium-enhanced barrier model. $\Delta H_t^‡$ values of 2.8, 3.1, 3.1, and 3.9 kcal/mol were found for TS, the two dialkylstilbenes, and DMS, respectively. Given that E_0 is expected to be a fraction of a kcal higher than $\Delta H_t^‡$, the TS value is in reasonably close agreement with the gas phase E_0 value of 3.4 ± 0.2 kcal/mol.[6] (For a discussion of the relationship between $\Delta H_t^‡$ and E_0, see refs 25 and 26.) In contrast, a large difference was found between $\Delta H_t^‡$ [27] and the estimated gas phase E_0[19] for DMS. For this comparison to be reliable, however, the value of E_0 should be derived by fitting the microcanonical rates to the predicted RRKM energy dependence, as will be done here.

In the present contribution, the full analysis of the supersonic jet work on MS, DMS, and PI is presented. RRKM calculations are carried out in an effort to quantify the reaction parameters for the isolated molecules and distill the essential vibrational and electronic effects of the substitutions. The study has also been extended to two additional *trans*-stilbene derivatives, by measuring the excess energy dependence of the photoisomerization rates of 4,4′-dihydroxy-*trans*-stilbene (DHS) and 1-(*trans*-*β*-styryl)cyclohexene (SCH). The first gives additional information on the role of the nature of the *para* substituent, while the second reflects the influence of the phenyl π conjugation on the electronic surfaces. The chemical structures of all the molecules studied are shown schematically in Figure 1. Spectroscopic analyses are reported of the low-energy vibrational structure in dispersed fluorescence of all of these molecules except DHS, in order to characterize the low-frequency vibrational modes which play a critical role in RRKM rates.

The rest of the paper is arranged as follows. The experimental setup and procedures are briefly described in section II. The experimental results of dispersed fluorescence spectra, IVR transients, and nonradiative decay rates are reported in section III. In section IV, the interpretation of the data is discussed, and the requisite information is developed to permit a comparison of the microcanonical rate measurements with RRKM theory. A discussion of structural effects on the photoisomerization dynamics is also presented. Section V summarizes the main conclusions of this work.

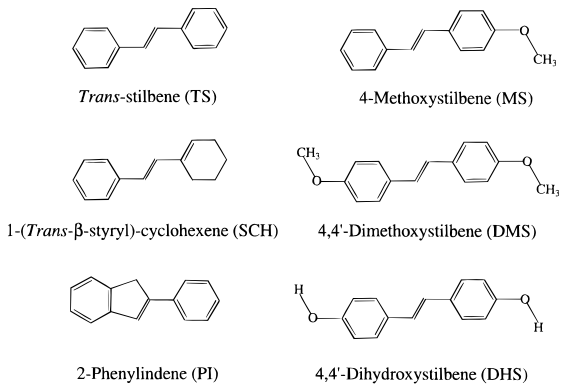

Figure 1. Chemical structures of the molecules studied.

II. Experimental Section

The technique of time-correlated single-photon counting of spectrally dispersed laser-induced fluorescence of jet-cooled molecules was employed. The methods and apparatus have been described elsewhere.[28,29] Here we give a brief description and report on aspects which are specific to this work.

II.1. Chemicals. *trans*-Stilbene (Aldrich, 96%), 4-methoxy-*trans*-stilbene (Parish), 4,4′-dimethoxy-*trans*-stilbene (Aldrich, 97%), and 4,4′-dihydroxy-*trans*-stilbene (ICN Biomedicals) were used without further purification. 2-Phenylindene was synthesized following the method described by Greifenstein *et al*.[30] NMR and mass spectra were taken to test the purity of the synthesized compound. The results of ^1H NMR ($CDCl_3$) are δ 7.1−7.7 (m, 10 H) and 3.8 (s, 2 H), which are in agreement with ref 31. 1-(*trans*-*β*-Styryl)cyclohexene was synthesized as described by Finley and Cable[32] and then purified by repeated vacuum sublimation until only a single peak remained visible by GC-MS (estimated purity >98%).

II.2. Jet Expansion and Laser Excitation. Helium (40−80 psi) was passed over the samples heated in a Pyrex tube and expanded through a ~60 μm pinhole in a continuous supersonic jet. The jet-cooled molecules were excited at a nozzle-to-laser distance of at least 25 times the pinhole diameter (X/D > 25) with the frequency-doubled output of a synchronously pumped, cavity-dumped picosecond dye laser system. The tuning element of the dye laser was a three-plate birefringent filter. To carry out the present work, the dyes DCM (1.5×10^{-3} M solution in a 3:2 (by volume) mixture of ethylene glycol and benzyl alcohol), R6G, and R110 (both 2×10^{-3} M in ethylene glycol) were used to cover the wavelength range from 550 to 666 nm. $LiIO_3$ and KDP crystals were used for frequency doubling. The resulting temporal and frequency pulse widths (fwhm) of the UV laser were ~15 ps and ~5 cm^{-1}, respectively.

II.3. Detection System. The laser-induced fluorescence (LIF) from the jet-cooled stilbenes was focused into the slit of a 0.5 m monochromator (Spex 1870) and detected by a Hamamatsu R2287U microchannel plate photomuliplier tube (PMT). The temporal data was measured using the time-correlated single-photon counting method.[33] The system response function had a full width at half-maximum (fwhm) of 60−90 ps.

The 0_0^0 transition band of TS[5] was used as the point of reference for absolute monochromator calibration, at the high resolution value of ref 34 (32 234.7 cm^{-1}). Frequencies reported in cm^{-1} have been corrected to vacuum. Excess vibrational energies for IVR and isomerization measurements are reported

TABLE 1: Energetics and Fluorescence Lifetimes of the S_1 Electronic Origin of *trans*-Stilbene Derivatives

molecule	$\lambda(0_0^0)$/Å	$\nu(0_0^0)^a$/cm^{-1}	$\Delta\nu^b$/cm^{-1}	τ_{fl}/ns
trans-stilbene (TS)	3101.4	(32 235)	0	2.61 (0.04)
4-methoxy-*trans*-stilbene (MS)	3250.4	30 757	−1478	2.97 (0.03)
4,4′-dimethoxy-*trans*-stilbene (DMS)	3334.0	29 986	−2249	2.96 (0.07)
2-phenylindene (PI)	3183.0	31 408	−827	3.17 (0.04)
4,4′-dihydroxy-*trans*-stilbene (DHS)	3283.4	30 448	−1787	3.57[c]
1-(*trans*-*β*-styryl)cyclohexene (SCH)	3010.8	33 204	+969	9.7 (0.7)

[a] The *trans*-stilbene origin at 32 234.74 cm^{-1} [35] was used as a calibration point. The other origin values result from addition of this value and the measured shifts (column 3). [b] Shift with respect to *trans*-stilbene 0_0^0 transition. The uncertainty is estimated at ±(5 cm^{-1} + 0.5%) for MS, DMS, and PI, ±50 cm^{-1} for DHS, and ±30 cm^{-1} for SCH. [c] One time measurement.

relative to the 0_0^0. When the correspondence of our measurements to bands in excitation spectra from other sources is clear, the values we believe to be most accurate are reported; otherwise, the approximate excess energy as determined at the time of the experiments is given. Due to changes in monochromator calibration, these are considered to have uncertainties of about ±30 cm^{-1}. The frequency-resolved measurements were not corrected for the spectral response of the detection system.

The 0_0^0 transitions of stilbene derivatives were located by manual scanning of the dye laser with the monochromator slit wide open and the detection wavelength fixed far to the red of the excitation laser wavelength. In this way, the reddest excitation band was considered to be the 0_0^0 transition. Excitation bands with more than ∼10% intensity relative to the 0_0^0 band were studied in the region where the excitation spectrum shows well-resolved features. At higher energy (the continuum region), the excitation wavelengths were chosen randomly.

II.4. Data Analysis. For the time-resolved fluorescence measurements, the measured decays were fit using the nonlinear least-squares method with Marquardt's algorithm accounting for convolution with the system response.[35] The values of the reduced χ^2 and the distribution of the residual indicated the goodness of the fit.

To characterize the dynamics of photoisomerization, time-resolved fluorescence measurements as a function of excess vibrational energy were recorded with wide-band detection centered at different wavelengths and under different experimental conditions.

III. Results

III.1. Molecular Symmetry and Notation. Studies of methoxybenzene (anisole) and its derivatives have established that the planar conformation of methoxy-substituted aromatics is favored.[36,37] A large number of experimental and theoretical investigations of anisole (refs 38−41 and references therein) have resulted in a fairly wide range of values, from ∼500 to ∼2000 cm^{-1}, for the height of the barrier to internal rotation of the methoxy group. It is expected, then, that for methoxy derivatives of TS, there will be two stable minima in each methoxy torsion potential, with the methyl carbon in the stilbene plane and the O−CH_3 bond *syn* and *anti*, respectively, to the orientation of the ethylene double bond. The two resultant conformers of MS have been identified by assignment of the excitation spectra[42] and measurement of rotational coherence recurrences.[43] For the two methoxy groups of DMS, three distinct conformers are expected (*syn,syn*-DMS, *syn,anti*-DMS, and *anti,anti*-DMS). The *syn*-MS and *syn,syn*-DMS conformers are represented in Figure 1. Hydroxy-substituted aromatics are also planar in the absence of steric hindrances (for example, phenol[44]), with a barrier to OH free rotation of ∼1200 cm^{-1},[45,46] so similar multiple conformations exist for DHS. The *syn,syn* conformation of DHS is shown in Figure 1.

trans-Stilbene has C_{2h} symmetry (considering the planar geometry[47−49]) with 72 vibrational normal modes. These normal modes are factorized into four symmetry groups: 25 a_g (ν_1−ν_{25}), 12 a_u (ν_{26}−ν_{37}), 11 b_g (ν_{38}−ν_{48}), and 24 b_u (ν_{49}−ν_{72}). The a_g and b_u modes are in-plane motions, while a_u and b_g are out-of-plane. All fundamental, overtone, and combination bands are allowed for the a_g modes, but only those overtones and combination bands resulting in a_g vibrational symmetry are allowed by the selection rules for the other symmetry species.

Symmetric (*syn,syn* and *anti,anti*) conformers of DMS and DHS also belong to the C_{2h} symmetry group, with 96 and 78 normal modes, respectively. MS (84 modes) and PI (75 modes), as well as *syn,anti*-DMS and -DHS, retain (at most) a plane of symmetry and therefore are classified in the symmetry group C_s, with a′ and a″ symmetry species. The correlation between symmetry species of C_{2h} and C_s is as follows: a_g and b_u correlate with a′ and b_g and a_u correlate with a″. Out-of-plane modes are of a″ symmetry, and therefore, as in TS, only even overtones of the out-of-plane modes in MS and PI are symmetry allowed in an allowed electronic transition. SCH is nonplanar[32] and thus belongs to symmetry group C_1, with no symmetry elements, and 84 modes of species a. Only one conformation of the torsion angle about the single bond between the styryl and cyclohexene moieties is seen in excitation, and this is assigned as *s-trans*,[32] as shown in Figure 1.

Because the symmetry and number of normal modes varies from molecule to molecule, a conventional scheme of numbering the modes would give six different numbers to a vibration of similar structural character in each of the molecules. Since we are interested in how the substituents and double-bond bridging affect the photoisomerization dynamics, our main concern regarding the vibrational mode assignments are the low-frequency modes, which play a dominant role in the vibrational state densities. In order to avoid confusion in the discussion of the substituent effect, we will adapt the approach of Siewert and Spangler[42] and designate similar vibrations in all molecules by the generally accepted mode numbering in TS. The eight modes of interest are the following: symmetric (ν_{25}, with a_g symmetry in TS) and antisymmetric (ν_{72}, b_u in TS) in-plane C_e−C_e−C_φ bends; the symmetric in-plane C_e−C_φ−C_φ bend (ν_{24}, a_g in TS); symmetric and antisymmetric C_e−phenyl torsion models (ν_{37}, a_u in TS and ν_{48}, b_g in TS); symmetric and antisymmetric out-of-plane phenyl bending modes (ν_{36}, a_u in TS and ν_{47}, b_g in TS), and the ethylenic torsion (ν_{35}, a_u in TS).[42,50,51]

We will refer to vibrational transitions as A_n^m, where A is the mode number and n and m are the number of quanta in the ground and electronic excited state, respectively. Combinations band are expressed as $A_n^m B_{n'}^{m'}$.

III.2. Spectroscopy. *III.2i. Excitation Spectra*. Table 1 summarizes the energetics of the S_1 electronic origins of all molecules as determined in this lab. Of the substituted stilbenes,

the only published excitation spectra are those of MS[42,52] and SCH.[32] In addition, Cable has recorded excitation spectra of MS, DMS, and PI.[53] The vibrational intervals in the MS spectra from the three available sources are in mutually good agreement, and the absolute frequencies reported for the lowest $S_1 \leftarrow S_0$ 0_0^0 transition (that of the *syn* conformer[42,43]), while varying somewhat more widely, confirm the MS origin assignment of ref 19 and of Table 1. Our previous assignments of the DMS and PI origins (ref 19 and Table 1) are likewise in agreement with the excitation spectra of Cable.[53]

The vibronic structure observed in SCH could be identified by reference to the published excitation spectra,[32] available prior to the work in this lab. The fluorescence excitation signal of DHS was very weak for all absorption bands, including the band assigned as the 0_0^0 transition. No LIF signal was observed when the laser wavelength was tuned further to the red. Our measurements of the origin band positions for these two molecules, as given in Table 1, have a larger uncertainty because a direct comparison with the TS origin was not made in these cases.

The low-energy vibronic structure in the excitation spectra of MS has been assigned previously.[42,52] Our interpretation and assignment are in closest agreement with that of Siewert and Spangler (SS).[42] The origin of the *anti* conformer of MS lies 279 cm^{-1} above that of the *syn* form. The low-frequency modes ν_{24}, ν_{25}, ν_{36}, and ν_{37} in S_1 are similar for the two conformers,[42] with all but ν_{37} being somewhat smaller than for TS, as expected from inertial considerations for modes entailing motion of the *para* ring position. The displacement of 25_0^1 to lower frequencies upon methoxy substitution in comparison with TS is in agreement with early work on MS in solution.[54,55]

The assignment of the 161 cm^{-1} band of *syn*-MS as 72_0^1, however, appears less certain. In TS, the calculated value of ν_{72}' is slightly below 100 cm^{-1},[16,50,56] and a frequency of 200 cm^{-1} has been assigned to 72_0^2 based on experimental isotopic shifts.[57] Like ν_{25}, a reduction of ν_{72} from TS to MS is expected, so a value of 161 cm^{-1}, while reasonable for 72_0^2, is unlikely for 72_0^1. As the fundamental of an in-plane vibration (b_u in TS), 72_0^1 becomes symmetry allowed with the change from C_{2h} to C_s symmetry, but how much strength it gains in absorption is uncertain. Therefore, it is possible that 72_0^1 is ~80 cm^{-1}. This reasoning may also be extended to the assignment of 72_0^1 in the 4-methyl-*trans*-stilbene excitation spectrum.[58] On the other hand, SS argue that a band observed at 67 cm^{-1} in *syn*-MS is not related to the methoxy group and is not dependent on the *para* substituent mass effect. This is also problematic, since only 72_0^1 among TS-like transitions not otherwise accounted for could reasonably be as low as 67 cm^{-1}, and in the absence of compensating force constant increases, it should also depend on the *para* substituent mass. Whatever is the correct assignment, we expect ν_{72}' to be below 100 cm^{-1}. (An alternative assignment[52] of the 161 and 67 cm^{-1} bands as hot, symmetry-forbidden transitions does not appear consistent with the data.)

No analysis of the excitation spectrum of jet-cooled DMS or PI has been carried out. Given the relative stabilization induced by the *syn* orientation of the methoxy group in S_1 MS, it is expected that the lowest origin among the conformers of DMS will be that of *syn,syn*-DMS. The probable *syn,anti*-DMS origin is a very strong band ~223 cm^{-1} higher than the *syn,syn*-DMS origin.[53] Above 400 cm^{-1}, the excitation spectrum is very congested, and a large number of strong bands between 455 and 540 cm^{-1} above the *syn,syn*-DMS origin are candidates for the origin of *anti,anti*-DMS. In the following section, dispersed fluorescence spectra of these bands will be discussed, and as in the case of MS, these permit a firm assignment of conformation in many cases. In the PI spectrum, the three strongest low-frequency transitions at 113, 148, and 281 cm^{-1},[53] when coupled with the dispersed fluorescence results below, are easily identified with the analogous transitions in TS of $36_0^1 37_0^1$, 37_0^2, and 25_0^1. The frequency changes from TS to PI are considered further in the following sections.

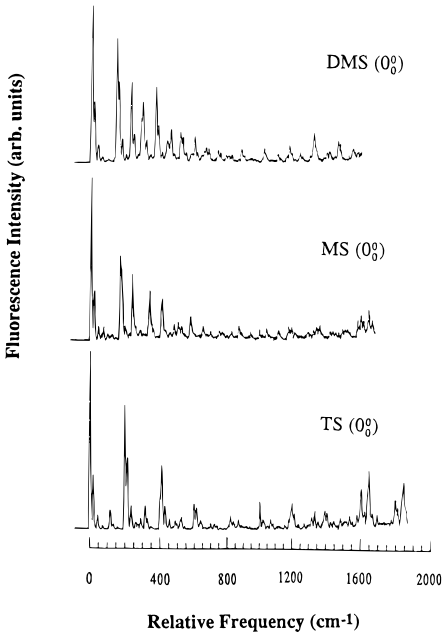

Figure 2. Dispersed fluorescence spectra of the S_1 0_0^0 levels of TS, MS, and DMS cooled in supersonic jet expansions. Experimental conditions for the three spectra, respectively: backing pressure *(P)* = 30, 40, and 40 psi of He; sample temperature *(T)* = 85, 115, and 145 °C; and nozzle-to-laser distance *(X)* = 3.2, 1.6, and 1.6 mm. The spectral resolution *(R)* was 0.5 Å for all three. *trans*-Stilbene data are shown for comparison. All plots are linear in wavelength, so the frequency axes are approximate.

The low-frequency structure in the SCH excitation spectrum[32] shows striking similarities with that of TS, although it is much weaker relative to the 0_0^0 transition than is the case in the latter molecule. Dispersed fluorescence spectra have been recorded for excitation of the most intense low-frequency bands, which we measure at excess energies of 0, 31, 95, and 192 cm^{-1}, in good agreement with the plotted spectra of ref 32. Using these as reference points, and with the effect of saturation[32] and the ground state intervals to help identify hot bands, all 26 observed bands below 225 cm^{-1} can be assigned using five modes analogous to ν_{25}, ν_{36}, ν_{37}, ν_{48}, and ν_{72} in TS. Of particular interest is the fact that the fundamentals of all these modes are observed due to the low molecular symmetry, although the four most prominent low-frequency vibrationally excited bands (seen at low laser fluence in Figure 6 of ref 32) are analogous to modes appearing prominently in the jet-cooled TS excitation spectra, as first fully assigned in ref 59: the 37_1^1 hot band (31 cm^{-1}), $36_0^1 37_0^1$ (91 cm^{-1}), 37_0^2 (95 cm^{-1}), and $25_0^1 \cong 37_0^4$ (192 cm^{-1}). This assignment places the four fundamentals 36_0^1, 37_0^1, 72_0^1, and 48_0^1 at 43, 47.5, 79.5, and 104.5 cm^{-1}, respectively. These vibrations have frequencies quite similar to their values in TS, the largest changes being a 20% increase in ν_{36}' and a 20% decrease in ν_{72}'.

III.2.ii. Dispersed Fluorescence Spectra. To more fully characterize the effects of substitution on the vibrational modes of these molecules, we have recorded and analyzed dispersed fluorescence spectra of their $S_1 \leftarrow S_0$ 0_0^0 transitions. TS, MS, and DMS dispersed fluorescence is shown in Figure 2, and that of PI and SCH is shown in Figure 3. The low-frequency mode

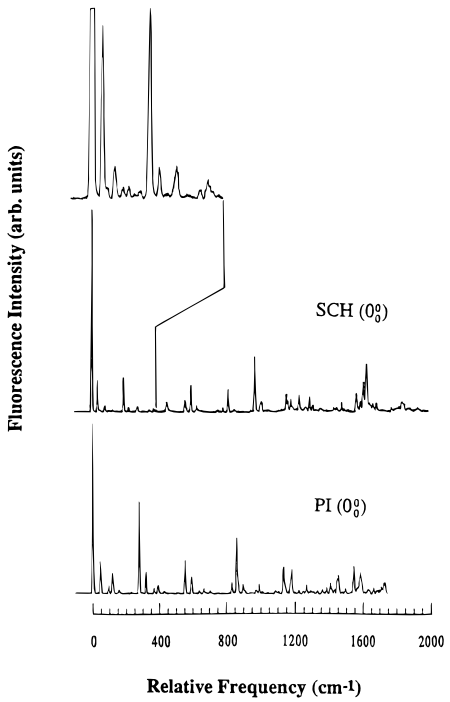

Figure 3. Dispersed fluorescence spectra of the S_1 0_0^0 levels of PI and SCH cooled in supersonic jet expansions (P = 40 and 30 psi of He; T = 105 and 95 °C; X = 1.6 and 1.6 mm; R = 0.5 and 0.8 Å, respectively). An expansion of the low-frequency region of SCH (up to 430 cm^{-1} above the 0_0^0 band) is also shown. All plots are linear in wavelength, so the frequency axes are approximate.

TABLE 2: A Comparison of S_0 Vibrational Frequencies (cm^{-1}) from Dispersed Fluorescence Spectra of Stilbene Derivatives

vibrational mode C_{2h} symmetry species	ν_{37} a_u	ν_{36} a_u	ν_{72} b_u	ν_{48} b_g	ν_{25} a_g	ν_{24} a_g
trans-stilbene	9.5	58		137	200	289
4-methoxy-*trans*-stilbene	9.5	46	59		166	237
4,4′-dimethoxy-*trans*-stilbene	7		48		143	227
2-phenylindene	23	58			283	
1-(*trans*-β-styryl)cyclohexene	18	63	53		196	287

assignments for all five molecules, which will be discussed below, are summarized in Table 2. Fluorescence from the assigned DHS origin was very weak, and its dispersed fluorescence spectrum was not recorded.

The assignment of the dispersed fluorescence spectra of TS is well documented, taking into account all the experimental and theoretical data available.[47,50,51,57,59−61] For comparison with our results for the derivatives, we give in Table 3 the vibrational intervals in the TS spectrum as determined from Figure 1. These are in close agreement (±(4 cm^{-1} + 0.5%)) with previously published values.[59−61] Assignment of almost all bands can be made[47,51] using only the modes ν_{24}, ν_{25}, ν_{36}, and ν_{37}. In a slight modification of the conclusion of ref 56, we assign the band at 274 cm^{-1} to 48_2^0, in accord with the assignment of the 229 cm^{-1} band in the excitation spectrum as 48_0^2.[57] ν_{72} has not been identified but is calculated at 85 cm^{-1} by Warshel.[50] (Note that, in Table 3 and the following tables, for each new mode that appears in an assignment the symmetry of the fundamental is indicated in parentheses.)

The dispersed fluorescence spectra of the lowest energy 0_0^0 transitions of MS and DMS (those of the *syn*-MS and *syn,syn*-DMS conformers) are similar in appearance to that of TS, and much of the prominent structure is readily assigned by simple correspondence. The band intervals and assignments for the low-frequency region are given in Tables 4 and 5. As with the excitation spectra, the MS dispersed fluorescence has been studied previously,[42,52] and our assignment follows the partial assignment of SS. We note that the variation among measured band intervals in Table 4 and refs 42 and 52 is larger than found when comparing the TS data of Table 3 to previous work. All intervals in Tables 3−7 were derived similarly and have comparable uncertainties.

The most prominent bands in the spectra of *syn*-MS and *syn,syn*-DMS, at 165 and 143 cm^{-1}, respectively, are assigned as 25_1^0. The change from TS is again qualitatively consistent with that observed in the fluorescence of MS and DMS in solution.[54,55] Similarly, from inertial considerations and the involvement of the *para* position in these motions, a successive lowering can be expected in MS and DMS of ν_{24}'', ν_{72}'', and ν_{36}'' from their values in TS. The assignments in Tables 4 and 5 have been made accordingly (see Table 2). The somewhat greater congestion in both MS and DMS dispersed fluorescence relative to TS is primarily attributed to much stronger activity of ν_{24}.[42]

As in the case of the excitation spectra, a reasonable assignment for the weak, low-frequency mode at 59 cm^{-1} in MS is 72_1^0, which becomes symmetry allowed with the change from C_{2h} to C_s symmetry. In *syn,syn*-DMS, in which C_{2h} symmetry is restored, 72_1^0 is forbidden, but the 97 cm^{-1} band is assigned to 72_2^0, since 72_2^0 and 36_2^0 in DMS are expected to lie below their values in MS of 119 and 92 cm^{-1}, respectively. Activity in ν_{36} then shows a consistent trend, being greatly reduced in MS and undetected in DMS. While ν_{37}'' changes little from TS to MS, its reduction in DMS may reflect the increased importance of the moment of inertia of the methyl groups about the phenyl torsion axes in the symmetric molecule.

Dispersed fluorescence was also recorded for many higher energy excitation bands of DMS. From the frequency and Franck−Condon pattern of the strong ν_{25}'' progressions, it is possible to assign the origins of the higher lying conformers. The value of 25_1 is 143 cm^{-1} at the lowest origin. At the +223 cm^{-1} band, it changes to ∼151 cm^{-1} and again to ∼160 cm^{-1} for excitation to a band at +475 ± 10 cm^{-1}. This last is probably the strong band at +471 cm^{-1} in the Cable excitation spectrum,[53] among a number of closely spaced bands from +470 to 486 cm^{-1}. In addition to this interval change, the Franck−Condon patterns of the bands at 0, 41, and 146 cm^{-1} are repeated at corresponding bands for the two higher origins. If we assume that the ordering of the origins follows that of MS, then the bands corresponding to 41 and 146 cm^{-1} in *syn,syn*-DMS are at 33 and 153 cm^{-1} in *syn,anti*-DMS and at ∼37 and ∼161 cm^{-1} in *anti,anti*-DMS. The Franck−Condon pattern in the emission spectrum of the higher vibration for each conformer has the distinctive characteristics of the 25_0^1 band of TS,[60] thus supporting the assignment. The direction of increase as a function of conformer of the frequency of ν_{25} (in both S_0 and S_1) is consistent with the conformation effect in MS.[24]

The analysis of the dispersed fluorescence of the PI origin (Figure 3) is reported in Table 6. Intramolecular bridging dramatically increases ν_{37}'' and ν_{25}'', modes which in TS entail significant relative displacement of the bridged carbon atoms. The increase in frequency is expected with the *freezing* of half the potential involved in the relative motion, which effectively lowers the reduced mass for the other *half* motion by almost a factor of 2. In contrast, ν_{36}'' is unchanged from TS, and the Franck−Condon activity in ν_{36} is very similar in PI and TS. In this mode, there are no large short-range distortions of the carbon backbone, with or without bridging. No band is seen which has an obvious correspondence to 24_1^0 in TS, and the complete assignment of bands up to 870 cm^{-1} uses only the three modes

TABLE 3: Assignment of S_0 Dispersed Fluorescence Spectrum (Low-Frequency Region) in *trans*-Stilbene

freq (cm^{-1})	int	assignt	freq (cm^{-1})	int	assignt
0	100	0_0^0	316	12	$25_1^0 36_2^0$
19	28	37_2^0 (a_u)	328	5	$25_1^0 36_2^0 37_2^0$
43	8	37_4^0	353	1	$25_1^0 36_2^0 37_4$
72	2	37_6^0	404 (sh)		$24_1^0 36_2^0$
115	13	36_2^0 (a_u)	413	39	25_2^0
132	4	$36_2^0 37_2^0$	432	13	$25_2^0 37_2^0$
156	1	$36_2^0 37_4^0$	454	6	$25_2^0 37_4^0$
200	70	25_1^0 (a_g)	489	6	$24_1^0 25_1^0$
214	40	$25_1^0 37_2^0$	500	4	$24_1^0 25_1^0 37_2^0$
235	13	$25_1^0 37_4^0$	525	6	$25_2^0 36_2^0$
264	6	$25_1^0 37_6^0$	604	17	25_3^0
274	4	48_2^0 (b_g)	618	15	$25_3^0 37_2^0$
289	7	24_1^0 (a_g)	641	6	$25_3^0 37_4^0$

TABLE 4: Assignment of S_0 Dispersed Fluorescence Spectrum (Low-Frequency Region) in 4-Methoxy-*trans*-stilbene

freq (cm^{-1})	int	assignt	freq (cm^{-1})	int	assignt
0	100	0_0^0	(258) (sh)		$24_1^0 37_2^0$
19	31	37_2^0 (a″)	283	8	$24_1^0 37_4^0$
42	9	37_4^0	337	31	25_2^0
59	5	72_1^0 (a′)	(357) (sh)	11	$25_2^0 37_2^0$
70	9	37_6^0	411	26	$25_1^0 24_1^0$
92	5	36_2^0 (a″)	429	8	$25_1^0 24_1^0 37_2^0$
119	5	72_2^0	457	6	$25_1^0 24_1^0 37_4^0$
141	2	$72_2^0 37_2^0$	479	11	24_2^0
166	53	25_1^0 (a′)	506	12	25_3^0
(178) (sh)		$25_1^0 37_2^0$	522	10	$25_3^0 37_2^0$
196	10	$25_1^0 37_4^0$	574	16	$25_2^0 24_1^0$
237	42	24_1^0 (a′)	652	10	$25_1^0 24_2^0$

TABLE 5: Assignment of S_0 Dispersed Fluorescence Spectrum (Low-Frequency Region) in 4,4′-Dimethoxy-*trans*-stilbene

freq (cm^{-1})	int	assignt	freq (cm^{-1})	int	assignt
0	100	0_0^0	315	15	$25_2^0 37_4^0$
14	39	37_2^0 (a_u)	338	6	$25_2^0 37_6^0$
36	12	37_4^0	368	49	$25_1^0 24_1^0$
59	4	37_6^0	384	24	$25_1^0 24_1^0 37_2^0$
97	3	72_2^0 (b_u)	405	8	$25_1^0 24_1^0 37_4^0$
143	79	25_1^0 (a_g)	433	15	25_3^0
154	52	$25_1^0 37_2^0$	454	22	24_2^0
175	16	$25_1^0 37_4^0$	475	7	$25_2^0 37_4^0$
197	6	$25_1^0 37_6^0$	511	20	$25_2^0 24_1^0$
227	52	24_1^0 (a_g)	527	17	$25_2^0 24_1^0 37_2^0$
243	19	$24_1^0 37_2^0$	544	7	$25_1^0 24_1^0 37_4^0$
268	6	$24_1^0 37_4^0$	574	7	25_4^0
(282) (sh)		25_2^0	596	18	$25_1^0 24_2^0$
292	39	$25_2^0 37_2^0$, 72_6^0			

TABLE 6: Assignment of S_0 Dispersed Fluorescence Spectrum (Low-Frequency Region) in 2-Phenylindene

freq (cm^{-1})	int	assignt	freq (cm^{-1})	int	assignt
0	100	0_0^0	515	1	$25_1^0 36_4^0$
46	17	37_2^0 (a″)	563	22	25_2^0
96	4	37_4^0	604	13	$25_2^0 37_2^0$
117	12	36_2^0 (a″)	650	2.5	$25_2^0 37_4^0$
157	2.5	$36_2^0 37_2^0$	677	4	$25_2^0 36_2^0$
233	1.2	36_4^0	715	3	$25_2^0 36_2^0 37_2^0$
283	63	25_1^0 (a′)	841	9	25_3^0
325	14	$25_1^0 37_2^0$	870	40	X_n^0
374	4	$25_1^0 37_4^0$	(880) (sh)	13	$25_3^0 37_2^0$
399	7	$25_1^0 36_2^0$	908	6	$X_n^0 37_2^0$
435	2	$25_1^0 36_2^0 37_2^0$			

ν_{25}, ν_{37}, and ν_{36}. The mode X which is introduced in the assignment of the higher bands is presumably outside the low-frequency range of principal interest here.

In the spectrum of SCH, the Franck−Condon intensity pattern is substantially altered from that of TS, beginning with a large dropoff in the intensity of the 25_n^0 and 37_{2n}^0 progressions and of 36_2^0 (Table 7). Nevertheless, assignment of the low-frequency region is fairly straightforward, and, consistent with the assignment of the excitation spectrum, most of the normal modes have frequencies very similar to their values in TS. Note that the symmetry species given in brackets in Table 7 would apply to the appropriate fundamentals for a planar structure. Of the five modes used, the only significant frequency shifts are in ν_{37}'' and ν_{72}'' (presumably). The ν_{36} and ν_{37} fundamentals are not seen, but this is not unexpected. The fundamentals of these modes were much weaker than the corresponding overtones in the excitation spectrum as well.[32] In the midfrequency range (>600 cm^{-1}), the spectrum here is cleaner than for the previous molecules, but prominent bands do not seem to fit a simple assignment scheme using only the above few modes and

TABLE 7: Assignment of S_0 Dispersed Fluorescence Spectrum (Low-Frequency Region) in 1-(*trans*-β-Styryl)cyclohexene

freq (cm^{-1})	int	assignt	freq (cm^{-1})	int	assignt
0	100	0_0^0	390	2	25_2^0
36	14	37_2^0 (a [a″])	470	6	$24_1^0 25_1^0$?
53 (sh)	0.5	72_1^0 (a [a′])	579	7	24_2^0, 25_3^0
80	3	37_4^0	617	13	X_n^0
106	0.7	72_2^0	658	4	$X_n^0 37_2^0$
126	1	36_2^0 (a [a″])	812	3	$X_n^0 25_1^0$
164	0.5	$36_2^0 37_2^0$, 72_3^0	845	12	Y_n^0
196	18	25_1^0 (a [a′])	879	2	$Y_n^0 37_2^0$
230	3	$25_1^0 37_2^0$	997	30	Z_n^0
287	4	24_1^0 (a [a′])	1033	7	$Z_n^0 37_2^0$
360	0.7	$25_1^0 36_2^0 37_2^0$			

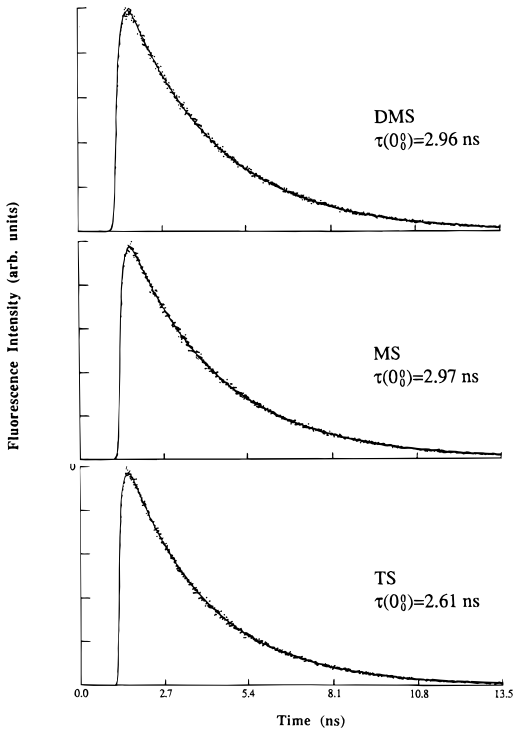

Figure 4. Fluorescence decays of the 0_0^0 transitions in TS, MS, and DMS with wide-band detection. Beam conditions are similar to those for Figure 1. The solid lines are the best fit, convoluted single-exponential functions ($\chi^2 \leq 1.1$). The average value of the fluorescence lifetime for each molecule is shown.

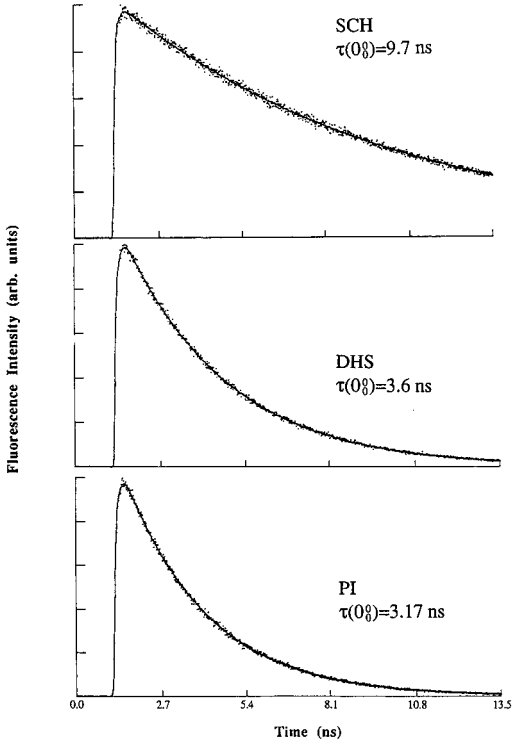

Figure 5. Fluorescence decays of the 0_0^0 transitions in PI, DHS, and SCH with wide-band detection (P = 40, 60, and 40 psi of He; T = 100, 210, and 100 °C; X = 1.6, 1.6, and 3.2 mm, respectively). The solid lines are the best fit, convoluted single-exponential functions ($\chi^2 \leq 1.0$). The average value of the fluorescence lifetime for each molecule is shown.

in which progression intensities decrease monotonically with the number of vibrational quanta. Therefore, the assignment in Table 7 is completed using three modes (labeled *X*, *Y*, and *Z*) which will be of no further concern here.

III.3. Dynamics. *III.3.i. Lifetimes of the 0_0^0 Transitions.* For each of the molecules studied here, time-resolved fluorescence has been measured a number of times exciting to the S_1 electronic origins listed in Table 1. Sample data are shown in Figures 4 and 5, plotted with the corresponding best fit single-exponential decay functions. For each molecule, except DHS, at least five such measurements were made, not all on the same day, and the average lifetime is given in the figure and reported in the last column of Table 1. The value in parentheses after the lifetime is the 90% confidence limit for Student's *t*-distribution. The large uncertainty in the SCH value stems from the fact that less than $1^1/_2$ fluorescence lifetimes were observed on the experimental time range employed in the measurements.

The lifetime of *syn*-MS has been confirmed by the recent measurement of Troxler *et al.*[43] The TS lifetime is in agreement with previously published values.[3−5,8] Absolute quantum yield measurements in TS[62,63] indicate that the lifetime at the origin corresponds to the pure radiative lifetime (τ_{rad}) and that the intersystem crossing channel is closed. Stilbene derivatives studied in this work show an increase in the fluorescence lifetime of the S_1 electronic origin in comparison with TS, which we take as an indication that the intersystem crossing can still be disregarded as a nonradiative channel, at least at low excess energy.

III.3.ii. Intramolecular Vibrational Energy Redistribution. Intramolecular vibrational energy redistribution (IVR) in TS has been studied before by picosecond time-resolved fluorescence measurements.[64] At low vibrational energies (<750 cm^{-1}, except for vibrational levels at 396^{29} and 663 cm^{-1}, which show quantum beats), IVR is absent, and fluorescence decays exponentially. Quantum-beat modulated decays are observed in the energy region 789−1170 cm^{-1}, revealing the existence of restricted IVR with recurrence times of several hundred picoseconds. Finally, at energies greater than ∼1200 cm^{-1}, biexponential decay behavior indicates dissipative IVR with IVR lifetimes, as determined from the fast components of the biexponentials, on the order of tens of picoseconds (20−50 ps).[64]

In order to characterize the effect of *para*-methoxy substitution and intramolecular bridging on IVR, and its possible role

in the isomerization process, a similar investigation has been carried out on MS, DMS, and PI. Fluorescence decays with single-band detection and dispersed fluorescence spectra have been measured for most vibronic transitions of significant intensity up to about 1400 cm^{-1} above the lowest electronic origin of each molecule. For MS and DMS, the actual excess vibrational energy of each transition depends on the specific conformer excited, but for the moment, the observations will simply be referenced to the lowest origin. The excitation energies for all molecules have been corrected from earlier values,[19] based on reanalysis with reference to the excitation spectra of Cable.[53]

Time-resolved fluorescence from single vibronic states reveals the absence of IVR (for our time resolution) for excitations below 0_0^0 + 640, 500, and 700 cm^{-1} in MS, DMS, and PI, respectively. Dispersed fluorescence spectra for prominent excitation bands at these energies are uncongested, and spectrally resolved fluorescence bands show single-exponential decay. By increasing the excitation energy, excitation bands are found in each molecule which give rise to quantum-beat modulated decays and some spectral congestion, revealing restricted IVR. For MS, strongly beat-modulated fluorescence decays were observed for two excitation bands, 673 and 913 cm^{-1} (see Figure 6), and some modulation for a third at 733 cm^{-1}. Two bands of DMS, at 530 and 955 cm^{-1}, gave rise to relatively pure, weakly modulated beating decays, and several bands show biexponential fluorescence decays with some modulation. One example of each type is shown in Figure 7. For PI, in the energy range of moderately congested dispersed-fluorescence spectra between 700 and 1000 cm^{-1}, two excitation bands, at 939 and 993 cm^{-1}, show well-modulated beating decays (Figure 8), and one other (709 cm^{-1}) shows weak modulation.

At still higher excitation energies, the temporal evolution of spectrally resolved fluorescence at wavelengths favorable to detection of structured emission can be characterized as predominantly biexponential in form. This is the case for bands in the range 821−1316 cm^{-1} in MS, 1006−1143 cm^{-1} in DMS, and 1106−1386 cm^{-1} in PI. Representative spectra and decays in this energy region are shown for the three molecules in Figures 9, 7, and 10, respectively. The biexponential fit parameters derived from many of these decays are listed in Table 8. The long-component lifetimes from the fits are consistent with the total-fluorescence-detection lifetimes, and the fast lifetimes are attributed to dissipative IVR. The corresponding dispersed fluorescence spectra of MS become very congested with little or no sharp structure (Figure 9a), as is the case for TS,[64] while the spectra of DMS and PI continue to have prominent sharp bands (Figures 7a, top, and 10a). The interpretation of this data will be discussed in section IV.1.

III.3.iii. Nonradiative Decay Rate. The fluorescence decay lifetimes of jet-cooled TS, MS, DMS, PI, DHS, and SCH were measured as a function of excess vibrational energy. In general, the time-resolved fluorescence shows single-exponential and detection-wavelength-independent decays. Repesentative data for each molecule excited to high excess energy are shown in Figure 11. In the energy range characterized by restricted IVR, the decays were not always well fit by single-exponential functions, and for SCH a second decay component of low absolute amplitude was detected at all energies. This is most probably attributable to an impurity. Uncertainties in the measured fluorescence lifetimes are estimated at ≤10%, except for those lifetimes which are comparable to the system response width, in which case they may be as large as 20%.

Using 0_0^0 fluorescence lifetime to approximate the radiative lifetime, τ_{rad}, the nonradiative decay rate constant (k_{nr}) may be

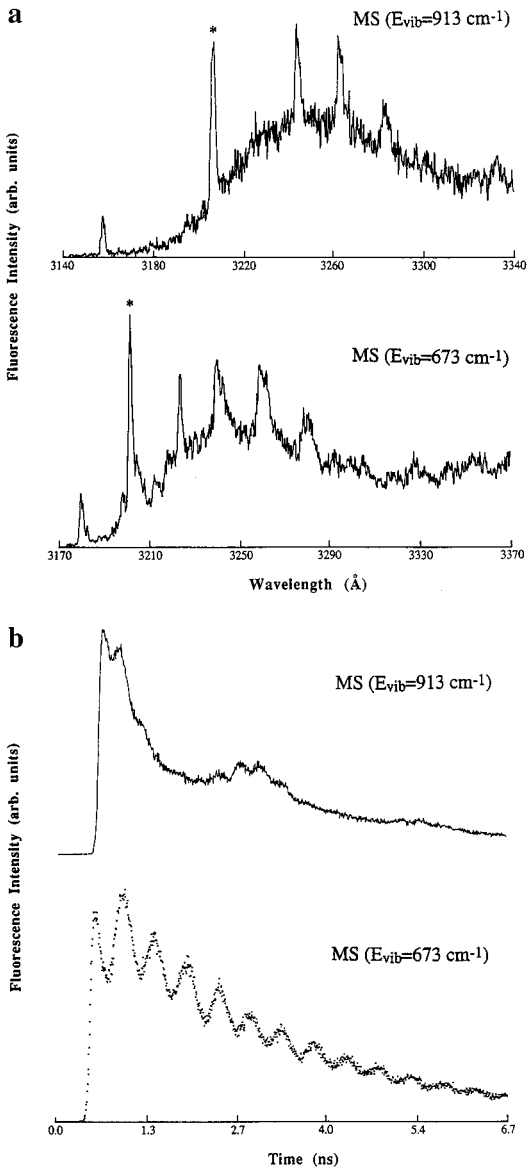

Figure 6. Restricted IVR in MS. Beam conditions: P = 70 psi of He, $T \sim$ 100 °C, and X = 1.6 mm. (a) The dispersed fluorescence spectrum of MS excited to photoselected vibrational levels (673 and 913 cm^{-1}) in the S_1 manifold. R = 1.6 Å for both spectra. (b) Time-resolved fluorescence measurements for the same excitation bands with single-band detection, R = 1.6 and 3.2 Å, respectively. The detection bands are identified by asterisk in (a). The recurrence times are estimated as 469 ps (673 cm^{-1}) and 300 ps and 1.93 ns (913 cm^{-1}).

calculated from τ_{fl}, the fluorescence lifetime as

$$k_{nr} = \tau_{fl}^{-1} - \tau_{rad}^{-1} \quad (1)$$

Absolute fluorescence quantum yield measurements of TS[62,63] indicate that the radiative lifetime is not constant and therefore that k_{nr} as given by eq 1 is only approximate. Measurements of this type are not available for the other molecules studied, so this refinement has not been considered in the present analysis. A plot of k_{nr} as a function of excess energy for all molecules is shown in Figure 12. The MS, DMS, and DHS rates have been plotted relative to the energy of their lowest electronic origin. Qualitatively similar behavior was observed for each molecule: the rate remains relatively constant at low energies and then rises smoothly as a function of energy above a characteristic energy threshold.

The data for isolated TS is in good agreement with that in the literature, as has been reexamined recently.[17] Figure 12

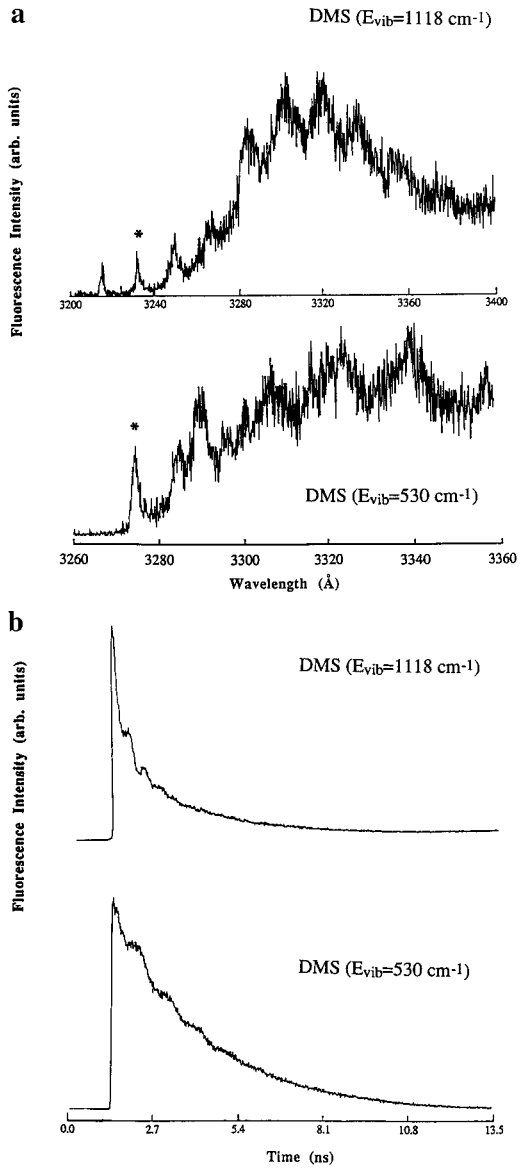

Figure 7. Restricted IVR in DMS. (a) Dispersed fluorescence spectra of S_1 + 530 and 1118 cm^{-1} vibronic levels. Beam conditions: P = 80 and 60 psi; T = 165 and 180 °C; X = 1.6 and 1.6 mm, respectively. R = 1.6 Å for both spectra. Note the shorter wavelength range for the 530 cm^{-1} spectrum, which has not been corrected for monochromator error. (b) Time-resolved fluorescence of the 530 and 1118 cm^{-1} vibrational levels. The detection bands are identified by asterisks, with R = 6.4 and 9.6 Å, respectively. X = 3.2 mm for the 530 cm^{-1} data; otherwise, beam conditions are the same as for the spectra. The recurrence times are estimated as 895 ps (530 cm^{-1}) and 468 ps (1118 cm^{-1}). There is a small contribution of scattered laser light at the peak of each decay.

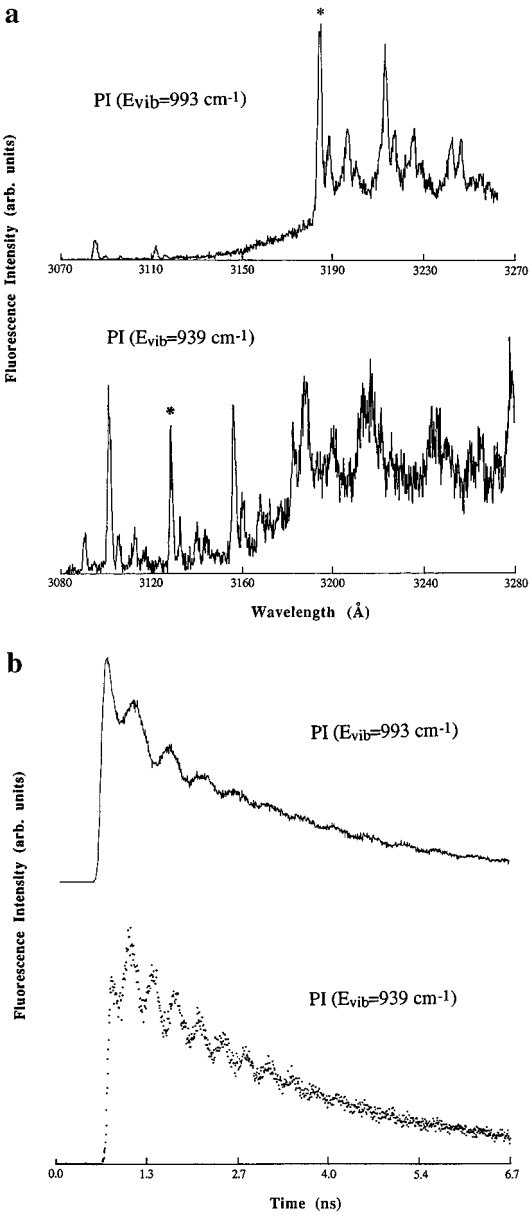

Figure 8. Restricted IVR in PI. Beam conditions are P = 70 psi He, T = 110 °C, and X = 1.6 mm. (a) Dispersed fluorescence spectra of PI excited to S_1 + 939 and 993 cm^{-1}. R = 1.6 Å for both. (b) Time-resolved fluorescence decays of the 939 and 993 cm^{-1} vibrational levels. The detection bands are identified by asterisks, with R = 1.6 and 1.3 Å, respectively. The recurrence times are estimated as 335 ps (939 cm^{-1}) and 488 ps (993 cm^{-1}).

shows the the behavior of MS is only slightly different from that of TS, while the rate slows dramatically in DMS, DHS, and PI and increases in equally dramatic fashion for SCH. These results will be examined in the next section.

IV. Discussion

IV.1. Normal Modes and Vibrational State Densities. In order to compare measured rates to theoretical expectations for the different molecules, a resonable approximation of the S_1 vibrational state density of each molecule is required. Our goal is to capture the qualitative effect of substitution on the state density, which will depend most strongly on changes in the lowest frequency modes. For this reason, we will take as our basis the calculated TS reactant and transition state frequencies of Negri and Orlandi[16] and use the above spectroscopic results to obtain approximate scaling factors to adjust the low-frequency modes.

In addition, each stilbene derivative has normal modes associated with the substituent atom groups, whose frequencies must be estimated. For derivatives of benzene,[65] substitution for one hydrogen of an hydroxy or methoxy group causes major changes in three benzene modes, which behave as local C−H modes for the displaced hydrogen. For each *para* substitution in the stilbene derivatives considered here, three TS ring C−H modes (one stretch and two bends, at ∼3100, 1400, and 1030 cm^{-1} [50,56]) are removed and replaced by frequencies characteristic of the new bond.

In determining the effect of substitution on TS-like modes, we will rely principally on the changes in ground state frequencies, as seen in dispersed fluorescence, to estimate the effect in S_1. To the extent that those changes are inertial effects,

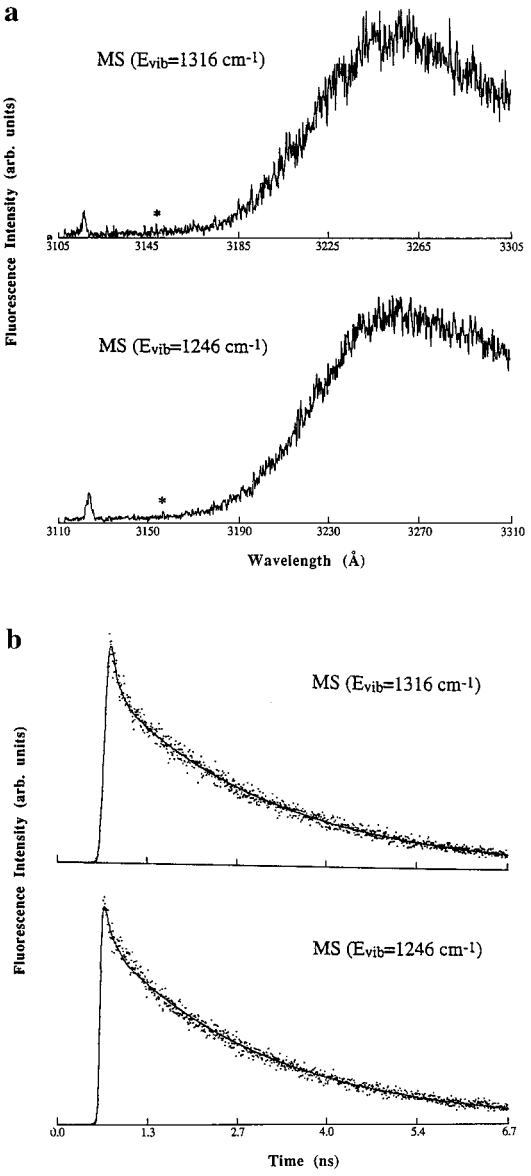

Figure 9. Dissipative IVR in MS. Beam conditions are $P = 70$ psi He, $T = 110$ °C, and $X = 1.6$ mm. (a) The dispersed fluorescence spectra of MS excited to 1246 and 1316 cm^{-1}, with $R = 2.4$ and 1.6 Å, respectively. (b) Biexponential fluorescence decays for the same excitation bands with single-band detection and $R = 16$ and 3.2 Å, respectively. The detection bands are identified by asterisks. The fitting parameters for 1246 cm^{-1} excitation are $\tau_1 = 39$ ps, $\tau_2 = 2.44$ ns, F/S = 2.2, and $\chi^2 = 1.06$ (results given in Table 8 are for a better fit to data of higher S/N), and for 1316 cm^{-1} excitation $\tau_1 = 55$ ps, $\tau_2 = 2.46$ ps, F/S = 1.96, and $\chi^2 = 1.0$.

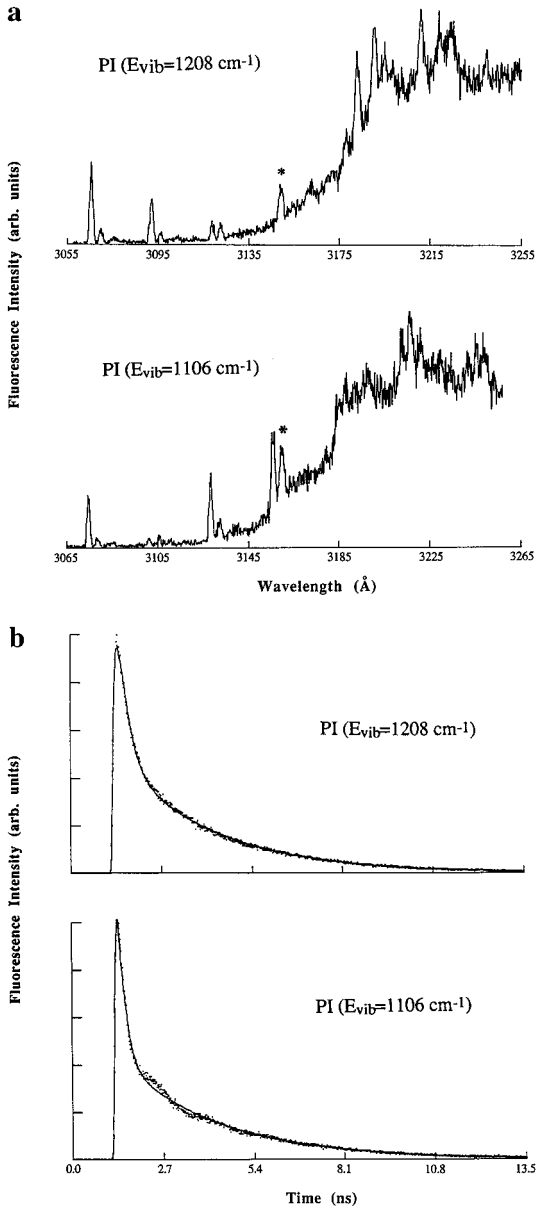

Figure 10. Dissipative IVR in PI. Beam conditions are $P = 70$ psi of He, $T = 110$ °C, and $X = 1.6$ mm. (a) Dispersed fluorescence spectra of PI excited to $S_1 + 1106$ and 1208 cm^{-1}, with $R = 1.6$ Å for both. (b) Biexponential fluorescence decays for the same excitation bands with single-band detection and $R = 1.6$ and 3.2 Å, respectively. The detection bands are identified by asterisks. The fitting parameters and $\tau_1 = 179$ ps, $\tau_2 = 3.0$ ns, F/S = 2.7, and $\chi^2 = 1.62$ for 1106 cm^{-1} excitation and $\tau_1 = 286$ ps, $\tau_2 = 2.9$ ps, F/S = 1.9, and $\chi^2 = 1.25$ for 1208 cm^{-1} excitation.

this approximation is valid, but substituent-induced changes in the vibrational potentials will be state specific. Therefore, we will use direct information about S_1 frequencies from the excitation spectra when possible.

The experimental values in Table 2 represent the low-frequency S_0 modes which account for all TS dispersed fluorescence bands below 300 cm^{-1}. In addition, the modes ν_{47} and ν_{35}, the ethylene torsion mode, are in the same frequency range and represent large scale motions of the entire molecular framework, so we will include them in the scaling. The remaining modes are more localized ring modes and C−H stretches and bends which are both higher in frequency and less sensitive to substitution, so will have less influence on the state densities.

From the comparison of MS and TS frequencies, we find a substitution-induced scaling of ∼0.8 for modes involving motion of the ring *para* position. A similar effect is deduced from the MS excitation spectrum,[42] particularly if the 161 cm^{-1} band is reassigned as 72_0^2. We therefore take 0.8 as the scaling factor for the five modes ν_{36}, ν_{72}, ν_{25}, ν_{24}, and ν_{35}. The C_e−phenyl torsion modes, ν_{37} and ν_{48}, are excluded, as is ν_{47}, which is essentially an out-of-plane deformation of the ethylene against the two phenyl rings. This is confirmed by the fact that the calculated deuteration effect on ν_{47} is much greater for deuteration of the ethylene hydrogens (TS-d_2) than for deuteration of the phenyl hydrogens (TS-d_{10}).[16]

For DMS, all frequencies in Table 2, including ν_{37}, are reduced from their values in MS, but the amount of the reduction varies substantially. For our calculations, we will approximate the DMS frequencies by scaling all eight low-frequency MS modes by a factor of 0.9.

TABLE 8: Dissipative IVR in 4-Methoxy-*trans*-stilbene, 4,4′-Dimethoxy-*trans*-stilbene, and 2-Phenylindene

molecule	E_v/cm^{-1}	ν_d[a]/cm^{-1}	τ_{slow}/ns	τ_{fast}/ps	F/S ratio[b]
MS	821	187	3.0	440	0.3
		557	2.8	440	0.1
	945	310	2.6	54	1.2
	1064	636	2.6	130	0.5
	1136	880	2.6	75	0.9
	1246	320	2.45	56	1.8
	1316	319	2.46	55	2.0
DMS	1006	183	3.0	330	1.3
		367	2.9	370	0.7
	1087	634	2.9	490[c]	0.8
	1118	160	2.45	180 ± 40[c]	2.1
		330	2.5	160 ± 60[c]	2.1
	1143	173	2.55	310	0.9
		345	2.6	220	1.1
PI	1106	556	2.8	160	5.3
		878	3.0	180	2.7
	1208	872	2.9	290	1.9
		1197	2.9	280	1.9
		1471	3.0	290	1.2
	1386	848	3.0	140	5.5

[a] Frequency shift of the detection band from the excitation energy. [b] Fast-to-slow component amplitude ratio. [c] Fitting parameters are sensitive to interaction of biexponential decay and quantum beat modulations.

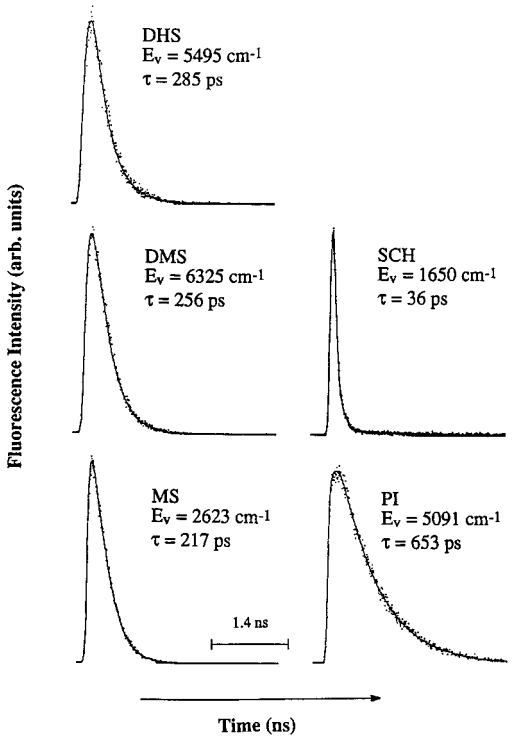

Figure 11. Time-resolved fluorescence decays at high excess energies in the S_1 state of MS, DMS, DHS, PI, and SCH. The excess energy and measured decay lifetime is given for each molecule. For SCH, in addition to the principal short-lived component, a minor second decay component (with a relative amplitude of 0.005) of lifetime 2.4 ns is observed.

Frequencies of modes associated with the methoxy group were estimated from experimental studies of methoxybenzene (anisole)[38,66] and a number of *para*-substituted anisoles.[38,67] The *para* substitutions are seen to have very little effect on most of the methoxy group vibrations. This holds true even for *p*-bromoanisole, in which the substituent mass (80 amu) approaches that of the corresponding substituent in MS. In a few cases there are distinct variations among the derivatives (e.g., a″ methyl rock, C−OCH_3 torsion), but reasonable

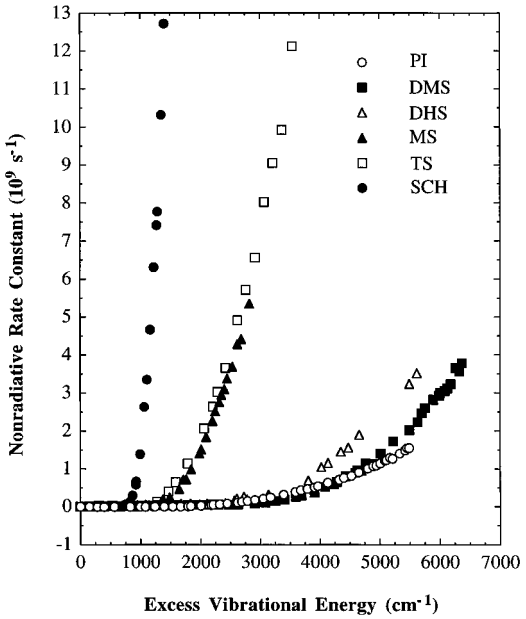

Figure 12. Excess energy dependence of the nonradiative rate constant in the S_1 manifold of jet-cooled TS, MS, DMS, PI, DHS, and SCH. The experimental data for SCH above 1400 cm^{-1} are not shown (see Figure 15).

TABLE 9: Methoxy Group Frequencies Used in Density-of-States Calculations for MS and DMS

mode description		freq/cm^{-1}
C−H stretch	antisymmetric a′	3000
	antisymmetric a″	2950
	symmetric a′	2830
C−H bend	antisymmetric a′	1450
	antisymmetric a″	1460
	symmetric a′	1440
O−CH_3 stretch		1030
methyl rock a′		800
methyl rock a″		1110
C−O−C bend		300
O−CH_3 torsion		200
C−OCH_3 torsion		80
C−O bond modes		
C−OCH_3 stretch		1240
C−OCH_3 bend, in-plane		500
C−OCH_3 bend, out-of-plane		245

estimates based on the experimental trends can be made. Descriptions of the 15 modes associated with the five methoxy atoms and their frequencies as used for the calculations for MS and DMS are given in Table 9. These 15 frequencies are added and three C−H modes removed for each methoxy group.

The excitation and dispersed fluorescence of methoxy-substituted benzenes[36] and stilbenes[42,52] do not show the tunneling splittings that are evident in *p*-methyl-*trans*-stilbene due to a low barrier to internal rotation of the methyl group.[58] This indicates that the barriers to methyl and methoxy free rotation in the methoxy species are much higher than the 100−200 cm^{-1} barriers to methyl rotation found in the methyl species. This ensures that the contributions of the torsional degrees of freedom to the calculation of state densities will be dominated by levels below the free rotation barriers. Therefore, the torsional modes will be treated as harmonic vibrations like all other modes.

In the spectra of SCH, most mode frequencies are very little changed from TS, as one would expect from inertial considerations only. But there is a large increase in ν_{37}'', revealing the effect of the change in conjugation. Because this change is

not an inertial effect, there is no reason to expect it to apply to S_1, and this is indeed the case. ν_{37}' is unchanged from TS to SCH, while ν_{36} increases about twice as much in S_1 (20%) as it does in S_0. At the same time, ν_{72}' decreases from TS to SCH. Due to the varying sign of the observed changes, we expect no significant net effect on the state density and assume a scaling factor of 1. The change of four phenyl hydrogens to eight aliphatic hydrogens in cyclohexene is approximated by removing four sets of aromatic C−H modes and adding eight sets of three aliphatic C−H modes (2960, 1450, and 1450 cm^{-1} [68]).

With no experimental information characterizing the vibrational modes of DHS, we can only estimate the inertial effect on the TS-like modes. The mass of the hydroxy group is over half that of the methoxy group, so we can lower the ∼30% frequency reductions in DMS to ∼30%/($2^{1/2}$) or ∼20% in DHS. Since OH has a very small moment of inertia about the $C_e-\varphi$ torsion axis, the two $C_e-\varphi$ torsions (ν_{37} and ν_{48}) are exempted from this effect. ν_{47} is also unchanged, for the same reason as noted for MS. Six C−H modes are removed, and two sets of hydroxy mode frequencies (3656, 1260, 1176, 408, 309, and 240 cm^{-1} [45,65]) are added.

Intermolecular bridging in PI causes a more fundamental change in normal mode structure than occurs in the case of substitutions. The effect of bridging on vibrations which in TS cause a relative displacement of the bridged atoms depends on the amplitude of that displacement and the nature of the mode. For example, symmetric TS modes which are essentially movements of one ring against the other (ν_{37} and ν_{25}) should retain similar forms in PI, but with deformation localized to the unbridged $C_e-\varphi$ bond. The mode frequencies rise, since the increase in force constant is dominant. Antisymmetric modes, which are ethylene vibrations against the inertia of the rings, are subject to large changes in both force constant and effective mass so may be severely distorted. The experimental data are very limited, since only three modes are seen in dispersed fluorescence. As a very rough approximation, the four symmetric phenyl−phenyl vibrations (ν_{37}, ν_{25}, ν_{24}, and ν_{35}) are scaled by 1.5, the average of the ν_{37} and ν_{25} changes in S_1, and the other modes are left unchanged. The three modes associated with the additional carbon are approximated by 900, 600, and 400 cm^{-1}.[68,69]

IV.2. The Substituent Effect on IVR. Since IVR is an important first step in the isomerization process, we have investigated this process in MS, DMS, and PI. The observation of quantum beats at a given excitation indicates that IVR is restricted at that excess energy, and vibrational energy remains relatively localized for at least the time scale of the recurrence period. However, recurrence periods fluctuate widely because they are proportional to the separations of a small number of randomly distributed coupled levels, and it is not easy to draw inferences from them on the global trends of IVR as a function of substituent. For this, it is more instructive to consider the characteristics of the dissipative IVR regime.

In a standard picture of dissipative IVR, the initially excited vibration is coupled to a relatively large bath of close-lying vibrational states, and the decay rate to the bath is proportional to the density of bath states (ρ) and depends on the strength of the vibrational coupling.[70] If the frequency sets described in section IV.1 are used to calculate vibrational state densities in S_1, one finds that the total density at the onset of dissipative IVR in TS (∼1240 cm^{-1}) is 300/cm^{-1}. The same total density is reached in MS, DMS, and PI at 850, 670, and 1390 cm^{-1}, respectively. ρ increases in MS and DMS by both the addition of methoxy modes and reduction in the frequencies of many TS-like modes, while the mode scaling is dominant in PI. It is possible, in addition, that the density of coupled levels in MS and PI is relatively higher than indicated by the calculations, due to the reduction in molecular symmetry of those molecules. These considerations lead unambiguously to an expectation that IVR will be enhanced in MS and DMS relative to TS. The effect in PI is not readily predicted, given the conflicting contributions of ρ and symmetry, especially since the density calculation is less reliable for PI than for the other molecules.

The onset of dissipative IVR is observed about 100 cm^{-1} lower in energy in PI than in TS, but the observed IVR rates, represented by the fast decay components of the biexponential decays given in Table 8, are from 5 to 10 times slower than those in TS, when compared at the same excess energies. Therefore, it is clear that the overall effect of intramolecular bridging has been to slow IVR somewhat. This implies that the estimated decrease in density is reasonable and that the effect of lowered symmetry on the coupling must be less significant than the density-of-states effect. Although IVR in PI is slower than in TS, the IVR rate below 1400 cm^{-1} (∼10^{10} s^{-1}) is still many times faster than the nonradiative rate measured at any energy in PI up to 5500 cm^{-1}.

Contrary to the observations for TS,[64] there is very prominent sharp structure in the PI spectra in the region of dissipative IVR (Figure 10). The sharp peaks arise from transitions of the initially prepared vibronic state, and therefore the relative yield of sharp to broad fluorescence reflects the competition between the IVR and radiative rates. For molecules with similar radiative rates, the fraction of sharp structure should be roughly proportional to the IVR lifetime. Thus, the relatively slow IVR rate of PI relative to TS accounts for the difference in spectral appearance.

In MS and DMS, an accurate characterization of IVR can be made only if the true vibrational energy content is known. In the MS assignment by SS,[42] most prominent bands above 279 cm^{-1} are attributed to *anti*-MS. In particular, the beating band at 0_0^0 + 673 cm^{-1} is assigned as *anti*-MS $25_0^1 24_0^1$. The other beating band at 913 cm^{-1} is the strongest band in its vicinity and thus is also likely due to *anti*-MS, possibly 24_0^3. Not only is the absorption of the *anti* conformer generally stronger than the *syn*, but the onset of IVR in *syn*-MS will further wash out its spectral structure and contribute to the dominance of peaks due to the *anti* form. Thus, it may reasonably be concluded that the occurrence of restricted IVR is actually for the range of vibrational energy content of ∼390−630 cm^{-1} in *anti*-MS.

By the same reasoning, the strong transitions for which decays were recorded in the dissipative IVR regime are also most likely due to *anti*-MS, at excess energies from ∼540 to 1040 cm^{-1}. In fact, the band at ∼820 cm^{-1} above the *syn*-MS origin is assigned by SS as the *anti*-MS 25_0^3 band, and comparison of the dispersed fluorescence spectrum recorded exciting this band with that of TS 25_0^3 [60] supports this assignment. The same range of energy in TS is clearly characterized by restricted IVR.[64] The trend with excess energy of the measured dissipative rates in MS (Table 8) is fairly smooth, with the exception of the fast rate at 945 cm^{-1}. This is a weak band in absorption[42,53] and may be due to the *syn* conformer. Assuming that all others are due to *anti*-MS, we see that the rates are slower than, but approaching, those measured in TS at ∼300 cm^{-1} higher excess energy. This result is in qualitative agreement with the simple vibrational state density argument given above, by which the IVR behavior in MS at ∼850 cm^{-1} should be comparable to that at 1240 cm^{-1} in TS.

The MS spectra in Figure 9 provide a further indication of the fast rate of IVR, as discussed in relation to PI. Here, there is no distinguishable sharp structure, with the peaks at the

excitation wavelength probably largely due to laser scatter. The lack of an isolated emission band for the detection of unrelaxed fluorescence may also contribute to the uncharacteristically small fast-to-slow amplitude ratio of the measured decays. When the intensity of relaxed emission within the detection bandwidth competes with that of the unrelaxed emission, the amplitude ratio will clearly be reduced from that associated with the time evolution of the optically active zeroth-order state.

In DMS, the assignment of bands to a specific conformer can be made as described in section III.2.ii. For example, the dispersed fluorescence of the beating band at +955 cm^{-1} displays a 160 cm^{-1} progression and can be confidently assigned to *anti,anti*-DMS 25_0^3, at an excess vibrational energy of ~484 cm^{-1}. In some cases, however, a clean assignment is difficult in light of the high spectral congestion, bandwidth of our laser, inadequate resolution in the dispersed fluorescence, or absence of the 25_n progression. Thus, *syn,anti*-DMS 25_0^2 (S_1 + ~306 cm^{-1} excess vibrational energy) should be at about +530 cm^{-1} above the lowest origin, but the Cable excitation spectrum shows a cluster of bands within 4 cm^{-1} of this value. The ground state interval in the fluorescence of the lower energy beating transition appears to correspond most closely to the 143 cm^{-1} value of *syn,syn*-DMS.

For the 1118 cm^{-1} excitation, as seen in the upper spectrum of Figure 7a, a progression of discrete bands appears at an interval of ~160 cm^{-1}. A weak band also appears ~160 cm^{-1} from the laser for 1087 cm^{-1} excitation. This is an indication that these bands arise in the *anti,anti*-DMS conformer at excess vibrational energies of ~647 and 616 cm^{-1}. The apparently longer interval in the weak dispersed fluorescence of the 1143 cm^{-1} band and the distinctly longer interval of a strong progression in the fluorescence of 1006 cm^{-1} band (see Table 8) leaves the conformational assignment of those excitations unresolved. However, as for MS, transitions of the higher energy conformers should dominate the strong discrete structure of the absorption spectrum above the onset of IVR, so the excess energies of these levels are also expected to be lower than the apparent energy by either 223 or 471 cm^{-1}. In any case, we observe dissipative IVR in DMS at much lower excess energies than in TS, but the onset of the dissipative behavior is apparently not lower than in MS. Thus, the higher symmetry of DMS may serve to moderate the effect of increased density of states on the IVR rate.

Although all the measured fast decay rates in DMS (see Table 8) are relatively slow compared to those in TS[64] and MS, the high level of congestion in the excitation spectrum due to the multiplicity of conformers could be a contributing factor. As discussed for MS, unrelaxed emission from vibronic levels with very fast IVR is intrinsically weak and is easily lost in the presence of sources of relaxed emission, such as would characterize the emission of the more stable conformers. Only excitations with slow IVR retain discrete structure of sufficient strength to be observed. For the next higher energy excitation band studied, at ~1240 or ~770 cm^{-1} in *anti,anti*-DMS, the measured dispersed fluorescence spectrum was completely diffuse, like those of MS in Figure 9a.

IV.3. Microcanonical Rates: Comparisons with RRKM Theory. The excess energy dependence of the *trans*-to-*cis* isomerization of isolated *trans*-stilbene may be very successfully represented over a wide energy range by nonadiabatic RRKM theory, which also provides a basis for explaining the greatly accelerated nonradiative decay rate in solution. The model for the reaction is that of an adiabatic pathway formed by crossing of the S_1 and S_n electronic state potentials as a function of ethylene twist angle.[13] (For discussion of the different versions of RRKM treatments see refs 6, 16, and 17.) We would like to see here whether the essential features of the structural effect on the photoisomerization dynamics can also be reproduced by this theory.

Briefly, the theoretical reaction rate, *k(E)*, is calculated using a modification of the standard RRKM expression to account for the Landau−Zener curve-crossing probability, *P*, that a nonadiabatic crossing of the transition state configuration will prevent reaction from occurring. The nonadiabatic rate is[6]

$$k(E) = \frac{\int_0^{E-E_0}(1-P)\rho^{\dagger}(E_V^{\dagger})\,dE_V^{\dagger}}{h\rho(E)} \qquad (2)$$

where *P* is given by

$$P = \exp\left[-\frac{\pi\gamma}{2\hbar\upsilon}\right] \qquad (3)$$

Here υ is the velocity along the reaction coordinate at the transition state, and $\gamma = \Delta^2/|F_1 - F_n|$, where Δ is the energy splitting of the adiabatic surfaces at the avoided crossing and F_1 and F_n are the slopes of the diabatic curves there. υ is calculated from the kinetic energy at the transition state and the reduced moment of inertia (I_{red}) for torsion about the ethylene bond. As γ increases, the reaction becomes increasingly adiabatic.

As a first level of approximation, the nonradiative decay of the substituted stilbenes (excluding PI) may be modeled by assuming that the effect of substitution is limited to a modification of the reactant and transition state vibrational-state-densities (ρ) and a relative shift of the S_1 and S_n states without otherwise affecting the nature of the reaction coordinate. The effect on ρ is given by the previously described spectroscopically motivated frequency adjustments (section IV.1), applied to the TS reactant and transition state vibrational modes. The energy shift will manifest itself in a change in reaction barrier height (E_0). Thus, by carrying out RRKM calculations like those previously applied to reproduce the TS reaction rate[6,16,17] and using E_0 as a fitting parameter, some insight may be gained into the influence of substitution on electronic structure. For PI, the *trans*-to-*cis* isomerization channel is closed, so a very different reaction coordinate and transition state must be involved. To compare with the results for the other molecules, nonadiabatic RRKM theory will also be applied to reproduce the measured energy dependence of the PI nonradiative decay rate.

In the case of MS, DMS, and DHS, the particular consequences of the existence of multiple conformers must be considered. We will focus here on the methoxy derivatives, since their properties are better established. First, we note that the data of Figure 12 show a single smooth dependence of k_{nr} *vs* energy above the lowest 0_0^0 transition for both MS and DMS. Since we know that transitions at the same laser wavelength result in excess energies in S_1 that differ by 279 cm^{-1} in MS and as much as 500 cm^{-1} in DMS for the separate conformers, the consistency of the rate trend at a resolution of ~100 cm^{-1} or less, coupled with the consistently excellent single-exponential fits of the decays, leads to the reasonable conclusion that only a single species is responsible for the observed decays.

One explanation for this observation could be the domination of a single conformer in the absorption spectrum. While it was reasoned that this interpretation is likely to apply to the intense sharp bands in the IVR region of the spectrum, it appears less plausible at energies where IVR in all conformers is very fast and the absorption spectrum forms a quasi-continuum. An

alternative explanation is that, at energies above the isomerization barrier, free interconversion of the conformers can take place on a time scale short with respect to isomerization, and the rate observed for absorption by any of the conformers is determined by the excess energy above the lowest excited state minimum.

The experimental rates in MS begin to rise perceptibly ~1100 cm^{-1} above the *syn*-MS origin. Therefore, for free interconversion to account for the smooth rate trend in MS, the torsion barrier must be lower than this value, which is in the lower half of the range of barrier energies cited for anisole.[38−41] (In anisole, the two minima are identical, but the barrier between unequal minima in MS and DMS should be of similar magnitude.) However, the fact that discrete structure is assignable to a specific conformer to above 900 cm^{-1} suggests that the torsion barrier is not much below 1100 cm^{-1}. In addition, for free interconversion to result in the observed smooth excitation energy dependence of the rate, the ground state zero-point levels of the conformers must lie very close in energy (ΔE < 50 cm^{-1}), for both MS and DMS. If this is the case, the spectral shifts between conformers are dominated by energy differences in the excited states. Calculations for MS and DMS, and also for DHS, are carried out under the assumption that the above conditions apply, and excess energies are measured relative to the lowest origin.

In the RRKM calculations for the substituted stilbenes, we will take as a point of reference a nonadiabatic calculation with γ equal to the value determined for TS (1.2 cm^{-1} rad)[16] and appropriate reduced moments of inertia (I_{red}) for each molecule. The vibrational frequencies are based on those of the *trans*-stilbene reactant and A transition state of Negri and Orlandi.[16] The A transition state arises at an avoided crossing of electronic state surfaces computed by the semiempirical QCFF/PI Hamiltonian including doubly excited configurations in the configuration interaction.[16] In all cases, it is found that essentially the same rate curves as are obtained using the A transition state with γ fixed at 1.2 cm^{-1} rad may also be derived from adiabatic RRKM calculations based on the B transition state, which is computed at a maximum on the S_1 surface, when doubly excited configurations are not included in the semiempirical calculation.[16] When a given energy dependence is not reproducible by this process, γ may also be varied to adjust the nonadiabatic calculation. This has a similar effect to changing the transition state frequencies, as has been used as a means of adjusting adiabatic RRKM calculations.[15] Thus, errors in the estimation of substitution effects on vibrational frequencies may result in apparent changes in γ in the fitting process.

The molecular structures needed to calculate I_{red} for the different molecules are derived from modifications to the structure of S_1 TS based on the calculations of Warshel[50] and rotational coherence measurements.[49] The rings are taken as coplanar in each case. The structure of the methoxy groups in MS and DMS was based on anisole,[71] and that of the hydroxy groups in DHS was based on phenol.[44,72] I_{red} for isomerization depends on conformation, but the effect of the differences on calculated rates is small compared to other uncertainties, so we will use the *syn* results in all cases. The values found for I_{red} for TS, *syn*-MS, *syn,syn*-DMS, *syn,syn*-DHS, and SCH are 262.8, 370.9, 630.0, 434.6, and 273.6 amu Å^2, respectively. The structure we used for MS accurately reproduces the experimentally determined[43] difference of the rotational constant sum, $B + C$, between *syn*-MS and *anti*-MS (experiment: $\Delta(B + C) = 4.6 \pm 0.6$ MHz; calculation: 4.54 MHz). The calculated $B + C$ for each conformer is ~0.6% lower than the measured value, which is within the absolute measurement accuracy.

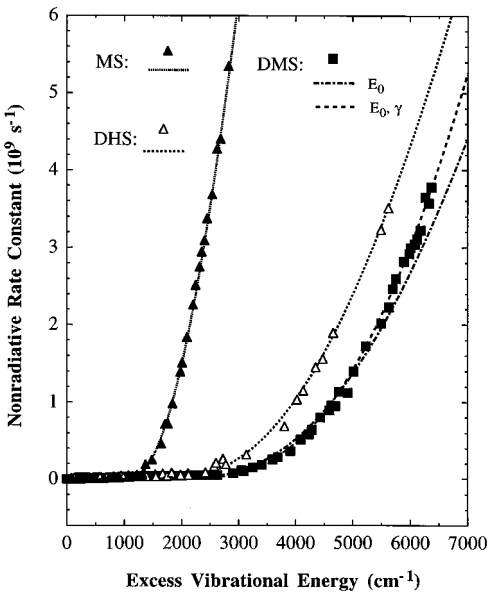

Figure 13. Comparison of experimental excess energy dependence of the nonradiative rate constant in MS, DMS, and DHS with nonadiabatic RRKM calculations. Calculation parameters for MS and DHS: $\gamma = 1.2$ cm^{-1} rad and $E_0 = 1110$ and 1700 cm^{-1}, respectively. For DMS, two calculations are shown, in which either only E_0 (with γ fixed at 1.2 cm^{-1} rad), or both E_0 and γ are varied. For the first, $E_0 = 1680$ cm^{-1}; for the second, the best fit is achieved for $E_0 = 1800$ cm^{-1} and $\gamma = 3.6$ cm^{-1} rad.

The effect of an increase in state density alone, with E_0 and γ fixed, is to slow down the rates compared to TS, though the reduction is somewhat moderated when I_{red} increases. At an excess energy of 3200 cm^{-1} (E_0 + 2000 cm^{-1}), the rate reduction is about a factor of 2 for MS, slightly less for DHS, and a factor of 3.4 for DMS. The calculated density in SCH does not change perceptibly from that of TS over the energy range considered, since the added C−H modes are relatively high in frequency.

Since the experimental rate for MS is higher, and those for DMS and DHS are lower than the rates calculated for the appropriate densities and E_0 fixed at the TS value of 1200 cm^{-1}, E_0 must be lowered for the MS calculation and raised for the DMS and DHS calculations, in order to match the data. It takes only a small change in barrier to produce a marked effect on the rates, and good matches to the rate behavior above the barrier can be achieved by adjustment of E_0 only, to 1110 and 1700 cm^{-1} respectively for MS and DHS. For DMS, a reasonable agreement, on the scale of the absolute measurement uncertainties, is also obtained by the single-parameter fit, for $E_0 = 1680$ cm^{-1}. In this case, however, a significantly better fit can be obtained by adjustment of γ also. E_0 and γ values for the best fit DMS calculation are 1800 cm^{-1} and 3.6 cm^{-1} rad. The calculated and measured rate constants are plotted together in Figure 13, with both the one- and two-parameter fits for DMS. Note that although the nonradiative decay of DHS is faster than that of DMS, when the same γ is used in the calculation, a slightly higher barrier is needed for DHS because of its lower state density.

To highlight significant features of the experimental and theoretical $k_{nr}(E)$ behavior at low excess energies which are not discernible in Figure 13, the calculated and measured time constants of MS, DMS, and DHS are plotted together in Figure 14. For each set of experimental data, most distinctly for DHS, there is a downward trend in measured lifetime at energies below the derived reaction barrier. This causes the data to clearly deviate from the theoretical curves, which are constant at the

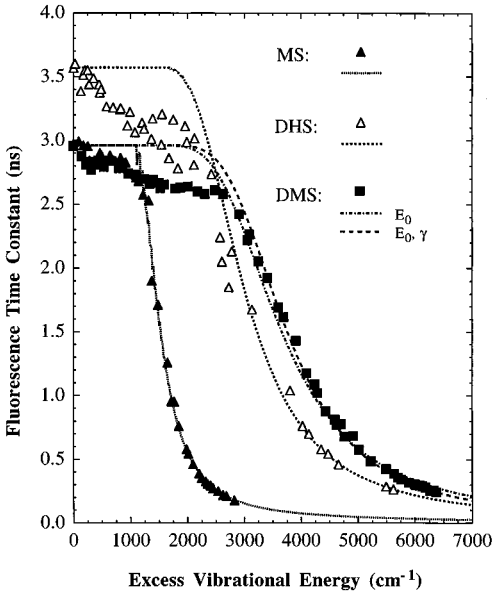

Figure 14. Nonadiabatic RRKM calculations and experimental excess energy dependence of fluorescence lifetime in MS, DMS, and DHS. Calculation parameters are the same as those given in the Figure 13 caption.

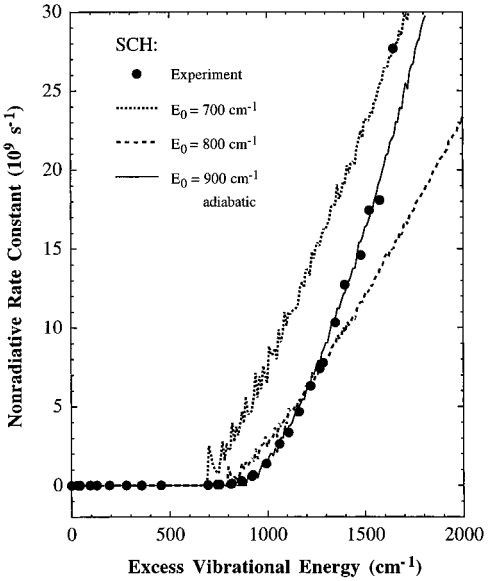

Figure 15. Excess energy dependence of the nonradiative rate constant (RRKM calculations and experimental measurements) in the S_1 state of SCH. $\gamma = 1.2$ cm^{-1} rad for the two nonadiabatic calculations (E_0 = 700 and 800 cm^{-1}).

origin lifetime in those energy ranges. This behavior appears to be related to the existence of multiple conformers for these molecules. For MS, the fluorescence lifetime is consistently shorter by ~0.1 ns above 279 cm^{-1}, *i.e.*, for excitations predominantly due to the *anti* conformer. Although 0.1 ns is not greater than the absolute lifetime measurement uncertainty, the consistent difference under the same experimental conditions is significant. This is supported by a similar difference seen previously in the lifetimes of the *syn*-MS and *anti*-MS origins.[43] A similar small change may occur at the 223 cm^{-1} band in DMS, which is apparently the *syn,anti*-DMS origin. Although the energetics of the DHS conformers are not known, the unambiguous drop in τ_{fl} at ~500 cm^{-1} may be supposed to indicate a higher energy origin in that region. (The scatter in DHS lifetimes in the energy range 1200−2400 cm^{-1} is probably due to variable systematic error in different experimental runs, rather than to a mode dependence of the decay rate.)

A second drop in DMS lifetime is seen at ~1000 cm^{-1}, to a plateau of ~2.65 ns. A similar drop is suggested in the MS data, but it is too close to the isomerization threshold to be clearly established. This we interpret to correspond to the onset to free methoxy rotation, which opens up access to the full range of conformations. The out-of-plane conformations apparently have higher radiative rates than the two planar ones or induce a weak nonradiative decay process. This effect may be responsible for the difficulty encountered in modeling the DMS solution data in ref 27. Here, the choice of the radiative rate used in the RRKM calculations also will affect the quality of the fit near and below the threshold, but the effect on the rates ($<0.05 \times 10^9$ s^{-1}) is negligible for high energies. Thus, the problem cannot have a large effect on the value of E_0 derived from the RRKM calculations, without a very large change in γ.

For both MS and DMS, the barrier required for the calculation is lower than the value of E_0 estimated previously from this data, by taking the energy at which a specific k_{nr} was surpassed.[19] This can be attributed primarily to the fact that the larger state densities make the rates near threshold increase more slowly, on the scale of the time resolution, than was the case for the reference molecule TS. This effect is quite large for DMS and is further enhanced by its higher barrier.

For SCH, acceleration of the decay rate begins at a lower energy, and leads to a steeper energy dependence, than for TS. A definite reduction in fluorescence lifetime begins by at least 743 cm^{-1} ($\tau_{fl} = 6.4$ ns) and possibly as low as 695 cm^{-1} ($\tau_{fl} =$ 8.0 ns). RRKM calculations with a variation of E_0 alone, or even with adjustment of γ, do not provide a satisfactory fit to the data over the entire energy range studied. One finds that the RRKM curves are rather linear given the low barrier and low state density, with an abrupt rise from the threshold. In contrast, the curvature of the experimental data is very large in the vicinity of 900 cm^{-1}. As shown in Figure 15, a completely adiabatic calculation with $E_0 = 900$ cm^{-1} is a fairly good match to experiment above 900 cm^{-1} but does not account for the steady fall in lifetime over the 200 cm^{-1} range below that energy (to ~2.6 ns by 866 cm^{-1}). Calculations with E_0 closer to the experimental threshold can approximate only a limited range of data, depending on the choice of E_0 and γ. For example, two plots for $\gamma = 1.2$ cm^{-1} rad and different values of E_0 (700 and 800 cm^{-1}) are shown in Figure 15.

Given the assumed frequency scaling factor of 1, the *calculated* state density in SCH is identical to that of TS until 1030 cm^{-1} (the first frequency affected by substitution), and it is known that IVR in TS is restricted in nature below an excess energy of ~1200 cm^{-1}. Therefore it is reasonable to expect IVR to be the rate-determining step in SCH isomerization over the first several hundred cm^{-1} range above the reaction barrier and consequently that the measured rate in this range will lie below the RRKM calculation. A dissipative IVR rate of ~30 $\times 10^9$ s^{-1} is measured in TS in the vicinity of 1240 cm^{-1}, a rate well above the measured k_{nr} in SCH at that energy. Therefore, if IVR occurs on a comparable time scale in SCH, it is not expected that IVR will remain a bottleneck in the SCH reaction much above this energy. The higher theoretical curve in Figure 15, with $E_0 = 700$ cm^{-1} and $\gamma = 1.2$ cm^{-1} rad, represents a calculation consistent with the apparent threshold and an IVR bottleneck which restricts the rate up to ~1500 cm^{-1}. At higher energy, the data should converge asymptotically to the energy dependence predicted by RRKM theory. For this picture to be correct, the IVR rate in SCH must be ~10 times lower than in TS.

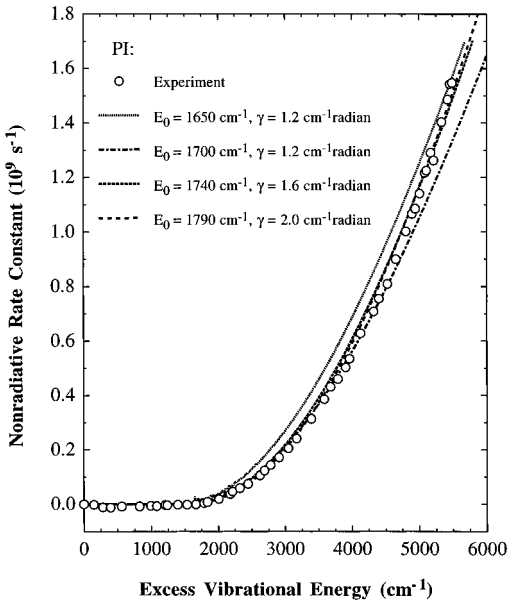

Figure 16. Experimental measurements and nonadiabatic RRKM calculations of the nonradiative rate constant, as a function of the vibrational energy, in the S_1 state of PI. RRKM calculations were repeated using one (E_0 = 1650 and 1700 cm^{-1}, with γ = 1.2 cm^{-1} rad) and two adjustable parameters (E_0 = 1740 and 1790 cm^{-1}, with γ = 1.6 and 2.0 cm^{-1} rad, respectively).

For PI, the reaction coordinate changes from the analogue of TS ν_{35} to ν_{37}. The calculated properties of the TS transition state are not applicable in this case, so we will use the reactant frequencies (scaled as described) with ν_{37} removed. The calculated reduced moment of inertia around the C_e-C_φ bond is 54.2 amu Å^2. As seen above, the state density of PI is lower than that of TS due to increases in vibrational frequencies, but the relative reduction of the transition state density (at equal E_0) is even greater because of the removal of ν_{37} and its replacement by a higher frequency. The nonadiabatic rate is further reduced by the much lower value of I_{red}. Thus, with no change in E_0 the calculated PI rate is about 4 times slower than that of TS, or actually slower than the comparable calculation for DMS in the 3000−4000 cm^{-1} excess energy range.

With the value of γ fixed at 1.2 cm^{-1} rad, nonadiabatic RRKM calculations can reproduce the measured rate behavior fairly well for a value of E_0 of ∼1680 cm^{-1}, but as for DMS, a better fit overall can be obtained by adjusting γ also. In Figure 16, the PI data are plotted with the results of four calculations, to indicate the sensitivity to the choice of parameters. For the best fit, the barrier is about 1770 cm^{-1}. Although, given the qualitatively different reactions of the two molecules, there is no reason to expect γ values in TS and PI to be closely related, γ remains in a fairly small range for a good fit to the entire range of data. Thus, as in TS, a good RRKM fit (with fixed frequencies) is only obtained far from the adiabatic limit, suggesting that the reaction barrier is due to an avoided crossing.

The values of E_0 for all the molecules studied are listed in Table 10. The barriers derived from the RRKM fits to the DMS, DHS, and PI supersonic jet data can be compared to barriers derived for these molecules in solution. The DMS barrier of 5.1 ± 0.2 kcal/mol corresponds to an increase with respect to TS of 1.7 ± 0.4 kcal/mol. From ref 27, the $\Delta H_t^‡$ value, derived from measurements in alkanes, is at most 3.9 kcal/mol for DMS, which is 1.1 kcal/mol higher than that for TS. Considering the uncertainties involved, these results are in reasonable agreement. The DHS barrier in polar solvents has been determined by analysis of isoviscosity plots[24] and compared to TS and DMS barriers derived by the same method.[22,23] The barrier was found to be from 0.2 to 0.6 kcal/mol lower in DHS than in DMS, a difference which is consistent with the comparable barriers determined here for these two molecules under isolated conditions.

TABLE 10: Nonradiative Process Thresholds for *trans*-Stilbene Derivatives

molecule	E_0[a]/cm^{-1}	molecule	E_0[a]/cm^{-1}
trans-stilbene	1220[b]	4,4′-dihydroxy-*trans*-stilbene	1700
4-methoxy-*trans*-stilbene	1110	1-(*trans*-β-styryl)cyclohexene	∼700[c]
4,4′-dimethoxy-*trans*-stilbene	1800	2-phenylindene	1770

[a] Derived from the best RRKM fit of $k_{nr}(E)$. The estimated uncertainty of ±70 cm^{-1} in the best fit value does not include consideration of uncertainties in the vibrational frequency sets used in the calculation. [b] This value is obtained using the TS data in Figure 12 with γ = 1.2 cm^{-1} rad. Previous nonadiabatic RRKM fits to a number of independent data sets[6,16,17] are all in agreement with E_0 = 1200 ± 100 cm^{-1}. [c] IVR limited non-RRKM rate behavior. Estimated upper limit.

The RRKM fit of the microcanonical rates yields a barrier for PI of ∼5.1 kcal/mol. This can be compared to an Arrhenius activation energy, E_a, of ∼10.2 kcal/mol determined for temperatures ranging from 374 to 473 K in hexadecane solution.[73] If the same set of solution rates is analyzed according to the expression for the solvent dependent enthalpy of activation, $\Delta H_{tp}^‡$, from ref 27, a value of $\Delta H_{tp}^‡ \sim$ 9.3 kcal/mol is found, compard to $\Delta H_{tp}^‡ \sim$ 4.7 kcal/mol for DMS in the same solvent.[27] Clearly, the difference between the isolated molecule barrier and solvated barrier is much more significant for PI (C_e-C_φ torsion) than for the double-bond twisting of the *para*-substituted stilbenes, possibly due to the solvent effect on the preexponential factors.

IV.4. Substituent Electronic Effects on Isomerization of Stilbenes. Substitutions in TS, such as methoxylation, represent perturbations to the molecular system that produce changes in the electronic wave functions of the molecule and thus in the potential energy surfaces for nuclear motion. Depending on the character of the substituent as weak or strong electron donor or acceptor, the PES's will be affected in different ways. The two main experimentally observed effects upon substitution in TS which are related to changes in the PES's are the energy shift in the S_1 electronic origin and the change, ΔE_0, in the isomerization threshold (barrier height). These both can be rationalized in terms of the model for isomerization involving crossing of the S_1 ($-L_a$ + E state) and the higher energy S_n ($+B_a$ state)[13] potential surface.

The observed red shift is understood when frontier orbitals are invoked. The electron-donating nature of the substituent indicates that the substituent orbital will effectively interact more strongly with the HOMO than with the LUMO of stilbene, simply because of the energy difference between HOMO and LUMO (the off-diagonal elements are the same). Figure 17a is a schematic representation of the interaction of the donor orbital, Φ_D, with the HOMO and LUMO. This type of picture has quantitatively accounted for substituent hyperconjugation probed in MCD (magnetic circular dichroism) studies.[74] The only blue shift observed, for SCH, reflects the decrease in the degree of conjugation. The stilbene L_a state is made of an extended delocalization over the ethylenic and phenyl π system, and as discussed by Michl[75] (for styrene and stilbene), the interaction between them leads to the lowering of S_1 energy (relative to ethylene) and to correlations along the reaction coordinate. (See ref 13 for the description of states involved.)

While the red shift of the excitation spectrum upon substitu-

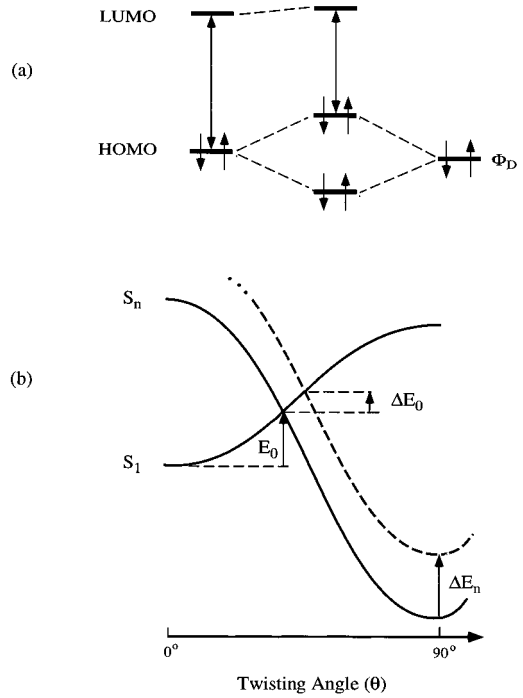

Figure 17. Electronic effects of substitution. (a) Energy level diagram illustrating the interaction of the HOMO of a donor substituent (Φ_D) and the HOMO and LUMO of the parent molecule. (b) Qualitative description of the change of effective potential energy curves as a function of the ethylene twisting angle θ, and the effect on the isomerization reaction barrier, E_0.

tion is due to the interaction with the stilbene HOMO in the planar configuration, the change in E_0 may be viewed roughly as the consequence of a differential effect of substitution on the S_1 and S_n potentials, while the shape and interaction of S_1 and S_n remain relatively unaffected. The fact that the energy dependence of k_{nr} for all the molecules studied (excluding PI and allowing for IVR limited rates in SCH) could be reasonably represented by RRKM fits with only one free parameter supports this hypothesis that the substituents do not fundamentally alter the nature of the reaction coordinate or transition state.

This description implies a simple relation between ΔE_0 and $\Delta E = \Delta E_n - \Delta E_1$, the shift in energy of S_n relative to S_1. Figure 17b is a representation of the S_1 and S_n potential surfaces as given by Hohlneicher and Dick,[13] illustrating the effect of such a shift, where, for simplicity, S_1 is assumed fixed. The change in barrier height is

$$\Delta E_0 = \Delta E \frac{F_1}{F_1 - F_n} \tag{4}$$

where F_1 and F_n are the slopes of the two surfaces, as before. Since ΔE_0 is measured, the unknown ΔE is given by $\Delta E = (1 - F_n/F_1)\Delta E_0$. When F_1 and F_n are of opposite sign, as shown, ΔE is larger in magnitude than ΔE_0 and of the same sign. For example, for $F_n \sim -F_1$, $\Delta E \sim 2\Delta E_0$, or for the case illustrated, $F_n \sim -2F_1$, $\Delta E \sim 3\Delta E_0$.

Assuming, for example, that the latter relation applies, the values of ΔE can be derived for each molecule. Although there are large uncertainties in F_1 and F_n, these do not affect the qualitative conclusions reached. From the reduced barrier for MS, one finds $\Delta E \sim -270$ cm^{-1}. Thus, S_n is slighly stabilized (relative to S_1) by one methoxy group. However, the addition of the second methoxy group raises $S_n \sim 1650$ cm^{-1} above its energy in TS. Thus the first and second methoxy groups have clearly opposite effects on the relative stability of the S_n state. The result for DHS of $\Delta E_n \sim 1500$ cm^{-1} is similar to but smaller than that for DMS.

The electronic structure effect on barrier height must reflect the nature of the transition state. The simple ethylenic twisting problem predicts, at 90° twisting, a diradical (DR) structure for the ground state and a *zwitterionic* (ZI) structure for the phantom state (the states of two electron systems). If the stilbene phantom state is ZI, then we expect the transition state for barrier crossing to have such character since the barrier is the result of the nonadiabatic coupling between the two potentials. According to this description, substitution effects change the barrier in well-defined directions.

The observed stabilization of the transition state relative to S_1 by the addition of one methoxy group is consistent with the fact that the OCH_3 group is electron donating (interacting with the HOMO) and stabilizes the ZI state by interacting with its positive charge center. On the other hand, with electron-donating groups on both rings, as for DMS and DHS, the ZI state cannot be favorably oriented with respect to the symmetrically higher electron density, thus resulting in the observed relative destabilization of the ZI state.

The SCH origin blue shift of 969 cm^{-1} is indicative of a destabilization of S_1 in comparison with TS. ΔE_n, the relative shift of S_n with respect to S_1, may be $\sim$2−3 times ΔE_0, or -1000 to -1500 cm^{-1}. The corresponding shift of S_n ranges from $\sim$0 to ~ -500 cm^{-1}. This suggests that the conjugation of the phenyl rings, which increases the stability of planar S_1 in TS by the overlap with the ethylene π orbitals, has little effect, or possibly a destabilizing effect, on the *zwitterionic* S_n state.

The above results elucidate the nature of the transition state and the reaction coordinate. The changes in E_0 and in the L_a state energies with substitution (by interaction with the HOMO) suggest the ZI character. As importantly, they indicate the care that must be taken if these reactions are studied in polar solvents. Here, in the isolated molecule the polarity effect is through the substitution, and in polar solvents similar effects may dominate, as discussed elsewhere.[23,24,76] Further studies in this laboratory will involve stepwise solvation of these substituted stilbenes, similar to the study reported earlier for stilbene with hexane.[77] The existence of a nonradiative channel in PI highlights the second important point regarding the dimensionality of the reaction coordinate. It appears that at least both the twisting and the torsion about the C_e-C_φ bond must be part of the global PES,[20,21,78] and our results on PI elucidate this point.

Finally, using the above picture, it is interesting to compare our model with other recent results on substituted stilbenes. A number of studies by Rettig and co-workers have focused on the dynamics of donor−acceptor substituted stilbenes and single- and double-bond bridged analogues, in solution[76,79−82] and in supersonically cooled samples.[83] One of these molecules, 4-(dimethylamino)-4′-cyano-*trans*-stilbene (DCS), has also been studied under jet-cooled conditions by Daum *et al.*[84] The donor−acceptor stilbenes have S_1-S_0 origins which are strongly red-shifted (from 4000 to 6000 cm^{-1}) and isomerization barriers lower than for TS. These characteristics are qualitatively consistent with the frontier orbital and ZI transition state picture. The red shift is large because, in addition to the interaction between the HOMO and the donor, interaction with the acceptor lowers the LUMO. The stability of the ZI state that is reflected in the lower barrier results from the interaction of the positive and negative charge centers of the ZI state with the polar charge distribution of the molecule.

The observation that single-bond bridging greatly decreases fluorescence quantum yield and increases rates in the donor−acceptor stilbenes in solution,[76,80] and leads to low barriers to

nonradiative decay in the jet-cooled samples,[83] has been postulated to support the existence of a fluorescent twisted intramolecular charge transfer (TICT) state resulting from twisting of the phenyl rings about the C_e-C_φ single bond. It should be noted, however, that a similar increase in rate is also observed for stiff stilbene (*trans*-1,1′-biindanylidene), the single-bond-bridged analogue of TS itself.[85,86] There is no indication in the well-studied spectroscopy of TS of any other low-energy pathway or fluorescent conformation contributing to its dynamics, so the rate-accelerating effect of bridging in stiff stilbene cannot be due to closing such a channel.

In the above discussion, the simple picture of a transition state formed by crossing of the S_1 and ZI S_n has been invoked.[9,13] New calculations of the electronic spectrum of *trans*-stilbene using multiconfigurational second-order perturbation theory[87] suggest that the barrier may result from crossing of the two lowest energy B_u states. In order to maintain the involvement of ZI character, we must include further crossings along the reaction coordinate and/or the multidimensionality of the twisting process. With the new level of accuracy achieved by theory,[87] we hope to be able to compare more quantitatively the theoretical and experimental findings for this series of stilbenes. Theoretically, the change of the potential energy along the twisting coordinates is needed, which is forthcoming.[87]

V. Conclusion

In this work we have studied structural effects on the isomerization dynamics of *trans*-stilbene, using picosecond time-resolved fluorescence spectroscopy. Intramolecular vibrational energy redistribution was characterized as well in several molecules and found to follow qualitatively the trends expected theoretically. The observed excess energy dependence of the isomerization process can in most cases be well represented by the same nonadiabatic RRKM theory previously applied to *trans*-stilbene, with only a change in the isomerization threshold energy required. The threshold energies extracted from the RRKM fits are related to the substituent effect on the relative positions of the two states involved in the nonadiabatic crossing leading to isomerization.

Intramolecular bridging in PI closes the isomerization channel (ethylenic double-bond twisting), and the observed threshold in the nonradiative decay rate constants is then associated with a different channel: the C_e-C_φ single-bond twisting. The energy dependence of the rate can also be well described by nonadiabatic RRKM theory, but in this case the deduced barrier is significantly lower than expected from rates measured in solution.[73]

These experimental and theoretical studies investigate the effect of electronic structure on the dynamics and should be applied also to other related systems.[81−83,88] The nature of the transition state elucidated here is important to studies in polar solutions and to the dynamics of barrier crossing. Further *ab initio* studies of the electronic states at different configurations should address the nature of the reaction coordinate.

Acknowledgment. We thank Dr. V. Alcazar for helping us in the synthesis of 2-phenylindene and NMR analysis and Mr. Hakno Lee for preparing the sample of 1-(*trans*-*β*-styryl)-cyclohexene. We also thank Prof. J. R. Cable for providing us with unpublished excitation spectra of several of the molecules studied, Prof. J. Michl for sending us his papers and for many stimulating discussions, and Prof. B. Roos for sending us his paper prior to publication. The helpful comments by the reviewers are greatly appreciated.

References and Notes

(1) Waldeck, D. H. *Chem. Rev.* **1991**, *91*, 415.
(2) Saltiel, J.; Sun, Y.-P. *Photochroism-Molecules and Systems*; Dürr, H., Bouas-Laurent, H., Eds.; Elsevier: Amsterdam, 1990; p 64.
(3) Syage, J. A.; Lambert, Wm. R.; Felker, P. M.; Zewail, A. H.; Hochstrasser, R. M. *Chem. Phys. Lett.* **1982**, *88*, 266.
(4) Majors, T. J.; Even, U.; Jortner, J. *J. Chem. Phys.* **1984**, *81*, 2330.
(5) Syage, J. A.; Felker, P. M.; Zewail, A. H. *J. Chem. Phys.* **1984**, *81*, 4706.
(6) Felker, P. M.; Zewail, A. H. *J. Phys. Chem.* **1985**, *89*, 5402.
(7) Rademann, K.; Even, U.; Rozen, S.; Jortner, J. *Chem. Phys. Lett.* **1986**, *125*, 5.
(8) Courtney, S. H.; Balk, M. W.; Phillips, L. A.; Webb, S. P.; Yang, D.; Levy, D. H.; Fleming, G. R. *J. Chem. Phys.* **1988**, *89*, 6697.
(9) Orlandi, G.; Siebrand, W. *Chem. Phys. Lett.* **1975**, *30*, 352.
(10) Tavan, P.; Schulten, K. *Chem. Phys. Lett.* **1978**, *56*, 200.
(11) Orlandi, G.; Palmieri, P.; Poggi, G. *J. Am. Chem. Soc.* **1979**, *101*, 3492.
(12) Olbrich, G. *Ber. Bunsen-Ges. Phys. Chem.* **1982**, *86*, 209.
(13) Hohlneicher, G.; Dick, B. *J. Photochem.* **1984**, *27*, 215.
(14) Khundkar, L. R.; Marcus, R. A.; Zewail, A. H. *J. Phys. Chem.* **1983**, *87*, 2473.
(15) Troe, J. *Chem. Phys. Lett.* **1985**, *114*, 241.
(16) Negri, F.; Orlandi, G. *J. Phys. Chem.* **1991**, *95*, 748.
(17) Baskin, J. S.; Bañares, L.; Pedersen, S.; Zewail, A. H. *J. Phys. Chem.* **1996**, *100*, 11920.
(18) Tahara, T.; Hamaguchi, H. *Bull. Chem. Soc. Jpn.* **1996**, *69*, 925.
(19) Bañares, L.; Heikal, A. A.; Zewail, A. H. *J. Phys. Chem.* **1992**, *96*, 4127.
(20) Park, N. S.; Waldeck, D. H. *J. Chem. Phys.* **1989**, *91*, 943.
(21) Park, N. S.; Waldeck, D. H. *Chem. Phys. Lett.* **1990**, *168*, 379.
(22) Zeglinski, D. M.; Waldeck, D. H. *J. Phys. Chem.* **1988**, *92*, 692.
(23) Sivakumar, N.; Hoburg, E. A.; Waldeck, D. H. *J. Chem. Phys.* **1989**, *90*, 2305.
(24) Park, N. S.; Waldeck, D. H. *J. Phys. Chem.* **1990**, *94*, 662.
(25) Sun, Y.-P.; Saltiel, J.; Park, N. S.; Hoburg, E. A.; Waldeck, D. H. *J. Phys. Chem.* **1991**, *95*, 10336.
(26) Saltiel, J.; Waller, A. S.; Sears, D. F., Jr.; Garrett, C. Z. *J. Phys. Chem.* **1993**, *97*, 2516.
(27) Saltiel, J.; Waller, A. S.; Sears, D. F., Jr.; Hoburg, E. A.; Zeglinski, D. M.; Waldeck, D. H. *J. Phys. Chem.* **1994**, *98*, 10689.
(28) Baskin, J. S.; Felker, P. M.; Zewail, A. H. *J. Chem. Phys.* **1987**, *86*, 2483.
(29) Semmes, D. H.; Baskin, J. S.; Zewail, A. H. *J. Chem. Phys.* **1990**, *92*, 3359.
(30) Greifenstein, L. G.; Lambert, J. B.; Nienhuis, R. J.; Fried, H. E.; Pagani, G. A. *J. Org. Chem.* **1981**, *46*, 5125.
(31) Bors, D. A.; Kaufman, M. J.; Streitweiser, A., Jr. *J. Am. Chem. Soc.* **1985**, *107*, 6975.
(32) Finley, J. P.; Cable, J. R. *J. Phys. Chem.* **1994**, *98*, 3950.
(33) O'Connor, D. V.; Phillips, D. *Time-Correlated Single Photon Counting*; Academic Press: New York, 1984.
(34) Champagne, B. B.; Pfanstiel, J. F.; Plusquellic, D. F.; Pratt, D. W.; van Herpen, W. M.; Meerts, W. L. *J. Phys. Chem.* **1990**, *94*, 6.
(35) Bevington, P. R. *Data Reduction and Error Analysis for the Sciences*; McGraw-Hill: New York, 1969.
(36) Oikawa, A.; Abe, H.; Mikami, N.; Ito, M. *Chem. Phys. Lett.* **1985**, *116*, 50.
(37) Breen, P. J.; Berstein, E. R.; Secor, H. V.; Seeman, J. I. *J. Am. Chem. Soc.* **1989**, *111*, 1958.
(38) Owen, N. L.; Hester, R. E. *Spectrochim. Acta* **1969**, *25A*, 343.
(39) Schaeffer, T.; Sebastian, R. *Can. J. Chem.* **1989**, *67*, 1148.
(40) Spellmeyer, D. C.; Grootenhuis, P. D. J.; Miller, M. D.; Kuyper, L. E.; Kollman, P. A. *J. Phys. Chem.* **1990**, *94*, 4483.
(41) Vincent, M. A.; Hillier, I. H. *Chem. Phys.* **1990**, *140*, 35.
(42) Siewert, S. S.; Spangler, L. H. *J. Phys. Chem.* **1995**, *99*, 9316.
(43) Troxler, T.; Topp, M. R.; Metzger, B. R.; Spangler, L. H. *Chem. Phys. Lett.* **1995**, *238*, 313.
(44) Larsen, N. W. *J. Mol. Struct.* **1979**, *51*, 175.
(45) Bist, H. D.; Brand, J. C. D.; Williams, D. R. *J. Mol. Spectrosc.* **1967**, *24*, 402.
(46) Quade, C. R. *J. Chem. Phys.* **1968**, *48*, 5491.
(47) Spangler, L. H.; van Zee, R. D.; Zwier, T. S. *J. Phys. Chem.* **1987**, *91*, 2782.
(48) Spangler, L. H.; van Zee, R. D.; Blankespoor, S. C.; Zwier, T. S. *J. Phys. Chem.* **1987**, *91*, 6077.
(49) Baskin, J. S.; Zewail, A. H. *J. Phys. Chem.* **1989**, *93*, 5701.
(50) Warshel, A. *J. Chem. Phys.* **1975**, *62*, 214.
(51) Urano, T.; Maegawa, M.; Yamanouchi, K.; Tsuchiya, S. *J. Phys. Chem.* **1989**, *93*, 3459.
(52) Chiang, W.-Y.; Laane, J. *J. Chem. Phys.* **1995**, *99*, 11823.
(53) Cable, J. R. Private communication.
(54) Bolotnikova, T. N.; Malkes, L. Y.; Nazarenko, A. I.; Yakovenko, V. N. *Zh. Prikl. Spektrosk.* **1968**, *9*, 858.
(55) Bolotnikova, T. N.; Malkes, L. Y.; Nazarenko, A. I.; Yakovenko, V. N. *Opt. Spektrosk.* **1969**, *26*, 649.
(56) Negri, F.; Orlandi, G.; Zerbetto, F. *J. Phys. Chem.* **1989**, *93*, 5124.

(57) Urano, T.; Hamaguchi, H.; Tasumi, M.; Yamanouchi, K.; Tsuchiya, S.; Gustafson, T. L. *J. Chem. Phys.* **1989**, *91*, 3884.
(58) Spangler, L. H.; Bosma, W. B.; van Zee, R. D.; Zwier, T. S. *J. Chem. Phys.* **1988**, *88*, 6768.
(59) Suzuki, T.; Mikami, N.; Ito, M. *J. Phys. Chem.* **1986**, *90*, 6431.
(60) Syage, J. A.; Felker, P. M.; Zewail, A. H. *J. Chem. Phys.* **1984**, *81*, 4685.
(61) Chiang, W.-Y.; Laane, J. *J. Chem. Phys.* **1994**, *100*, 8759.
(62) Amirav, A.; Jortner, J. *Chem. Phys. Lett.* **1983**, *95*, 295.
(63) Miller, C. C.; Hewett, K. B.; Shen, M. H.; Philips, L. A. *J. Chem. Phys.* **1995**, *102*, 145.
(64) Felker, P. M.; Lambert, Wm. R.; Zewail, A. H. *J. Chem. Phys.* **1985**, *82*, 3003.
(65) Versanyi, G. *Assignments for Vibrational Spectra of Seven Hundred Benzene Derivatives*; Wiley: New York, 1974.
(66) Balfour, W. J. *Spectrochim. Acta* **1983**, *39A*, 795.
(67) Goel, R. K.; Agarwal, M. L. *Spectrochim. Acta* **1982**, *38A*, 583.
(68) Herzberg, G. *Molecular Spectra and Molecular Structure*; Van Nostrand Reinhold: New York, 1945; Vol. II, p 195.
(69) Herzberg, G. *Molecular Spectra and Molecular Structure*; Van Nostrand Reinhold: New York, 1945; Vol. II, p 363−4.
(70) Tric, C. *Chem. Phys.* **1976**, *14*, 189.
(71) Onda, M.; Toda, A.; Mori, S.; Yamaguchi, I. *J. Mol. Struct.* **1986**, *144*, 47.
(72) Berden, G.; Meerts, W. L.; Schmitt, M.; Klienermanns, K. *J. Chem. Phys.* **1996**, *104*, 972.
(73) Dutt, G. B.; Konitsky, W.; Waldeck, D. H. *Chem. Phys. Lett.* **1995**, *245*, 437.
(74) Weeks, G. H.; Adcock, W.; Klingensmith, K. A.; Waluk, J. W.; West, R.; Vasak, M.; Downing, J.; Michl, J. *Pure Appl. Chem.* **1986**, *58*, 39.
(75) Michl, J.; Bonacic-Koutecky, V. *Electronic Aspects of Organic Photochemistry*; Wiley: New York, 1990.
(76) Rettig, W.; Majenz, W.; Herter, R.; Létard, J.; Lapouyade, R. *Pure Appl. Chem.* **1993**, *65*, 1699.
(77) Heikal, A. A.; Chong, S. H.; Baskin, J. S.; Zewail, A. H. *Chem. Phys. Lett.* **1995**, *242*, 380.
(78) Lee, M.; Haseltine, J. N.; Smith, A. B.; Hochstrasser, R. M. *J. Am. Chem. Soc.* **1989**, *111*, 5044.
(79) Rettig, W.; Majenz, W. *Chem. Phys. Lett.* **1989**, *154*, 335.
(80) Rettig, W.; Majenz, W.; Lapouyade, R.; Haucke, G. *J. Photochem. Photobiol. A: Chem.* **1992**, *62*, 415.
(81) Monte, Ch.; Hoffman, K.; Siemoneit, A.; Staak, M.; Zimmermann, P.; Rettig, W.; Lapouyade, R. Work to be published.
(82) Létard, J.; Lapouyade, R.; Rettig, W. *Mol. Cryst. A* **1993**, *234*, 581.
(83) Lapouyade, R.; Kuhn, A.; Létard, J.; Rettig, W. *Chem. Phys. Lett.* **1993**, *208*, 48.
(84) Daum, R.; Hansson, T.; Nörenberg, R.; Schwarzer, D.; Schroeder, J. *Chem. Phys. Lett.* **1995**, *246*, 607.
(85) Saltiel, J.; D'Agostino, J. T. *J. Am. Chem. Soc.* **1972**, *94*, 6445.
(86) Rothenberger, G.; Negus, D. K.; Hochstrasser, R. M. *J. Chem. Phys.* **1983**, *79*, 5360.
(87) Molina, V.; Merchán, M.; Roos, B. O. To be published.
(88) Létard, J.; Lapouyade, R.; Rettig, W. *Chem. Phys.* **1994**, *186*, 119.